UNIVERSITÀ DEGLI STUDI DI PADOVA

DIPARTIMENTO DI BIOLOGIA

Corso di Laurea magistrale in Molecular Biology

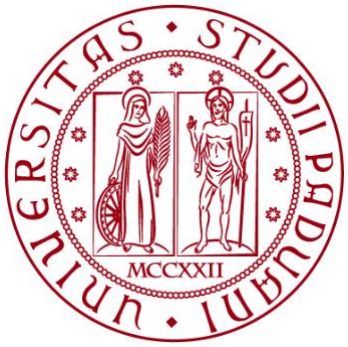

TESI DI LAUREA

Tau aggregates in neurodegenerative diseases: cause or consequence of autophagic dysfunction?

Relatore:
Prof.ssa Chiara Rampazzo
Dipartimento di Biologia, Padova

Correlatore:
Dott. Christel Brou
Institut Pasteur, Paris

Laureanda:
Eloisa Turco

ANNO ACCADEMICO 2021/2022

Ad Andrea, Elena, Linda,

Lucia, Michela e Gaia.

RIASSUNTO

Le taupatie, come l'Alzheimer (AD), la demenza frontotemporale (FTD), la paralisi sopranucleare progressiva (PSP) e la degenerazione corticobasale (CBD), sono malattie neurodegenerative caratterizzate da un anomalo accumulo di aggregati insolubili della proteina Tau. In tutte le taupatie gli aggregati possono propagarsi nel cervello in modo stereotipato e seguendo un meccanismo simile ai prioni. Inoltre, diverse taupatie sono caratterizzate dal malfunzionamento dell'autofagia, il principale sistema di rimozione di organelli danneggiati, proteine mal ripiegate, e di aggregati proteici. In particolare, la degradazione degli aggregati proteici è chiamata aggrefagia. In questo meccanismo, le proteine aggregate sono riconosciute da recettori altamente selettivi, come p62 e TAX1BP1, che interagiscono con LC3-II posizionato sugli autofagosomi, vescicole a doppia membrana che inglobano gli aggregati e li consegnano ai lisosomi per la degradazione. Tuttavia, resta da chiarire quale sia la relazione tra l'accumulo di aggregati di Tau e la compromissione dell'autofagia nelle taupatie.

Durante il mio tirocinio, ho indagato se gli aggregati di FL-Tau influenzano il flusso e l'attività autofagica, e se sono potenziali substrati dall'autofagia. Come modello neuronale, ho usato la linea cellulare SH-SY5Y di neuroblastoma umano che esprime gli aggregati di FL-Tau1N4R (P301S) marcati dalla proteina fluorescente mclover3. Per capire se FL-Tau nella sua forma solubile o insolubile influenza il flusso autofagico, ho monitorato attraverso immunoblot e analisi confocale i livelli di LC3-II e p62 in presenza e in assenza di bafilomicina, un inibitore autofagico. Successivamente, ho preparato gli estratti cellulari e separato il materiale solubile da quello insolubile (compresi gli aggregati) per valutare la stabilità degli aggregati di FL-Tau mediante immunoblot, in condizioni in cui la sintesi de-novo di FL-Tau solubile era compromessa. Infine, per vedere se gli aggregati di FL-Tau sono riconosciuti come materiale degradabile dall'autofagia, ho valutato attraverso immunofluorescenza (IF) la loro colocalizzazione con i recettori p62 e TAX1BP1, con gli autofagosomi marcati dalla proteina LC3 e con i lisosomi marcati dalla proteina LAMP1.

I risultati di immunoblot e dell'analisi confocale hanno dimostrato che nelle cellule SH che esprimono o mancano di aggregati FL-Tau i livelli di p62 e LC3

differivano in presenza e in assenza di Baf, suggerendo presenza di autofagia. Inoltre, le cellule SH contenenti FL-Tau sia nella sua forma solubile che insolubile sembrano non mostrare alcuna differenza nell'attività autofagica rispetto alle cellule SH che esprimono solo la proteina solubile. In più, dal saggio della stabilità è emerso che l'emivita di FL-Tau solubile e insolubile è di circa un giorno e che nel corso tempo gli aggregati di FL-Tau non sono presenti. Infine, dall'analisi di IF sembra che gli aggregati di FL-Tau possono essere riconosciuti dai recettori p62 e TAX1BP1, ma la loro degradazione autofagica non viene portata al termine.

In conclusione, i miei dati suggeriscono che gli aggregati di FL-Tau non alterano né il flusso né l'attività autofagica e che sono potenzialmente degradati nel tempo, ma in maniera indipendente dall'autofagia. Inoltre, i miei risultati evidenziano l'importanza di sviluppare un modello affidabile per approfondiare la relazione tra gli aggregati di Tau e i difetti autofagici nelle taupatie.

Table of contents

1. ABSTRACT

Tauopathies are neurodegenerative diseases, with Alzheimer's disease (AD) being the most common one, all characterized by abnormal accumulation of insoluble Tau aggregates. These latter propagate in patients' brain in a stereotypical manner following a prion-like mechanism and cause movement disorders, dementia, and cognitive decline. Several tauopathies share defects in the autophagy-lysosomal system, the primary route for clearance of protein aggregates. Upon receptors recognition, aggregates are engulfed by autophagosomes, that eventually deliver them to lysosomes for degradation. However, it remains to be elucidated whether accumulation of Tau aggregates is the cause or the consequence of autophagic impairment in tauopathies, and whether Tau aggregates can be degraded by autophagy in physiological condition.

During my internship, a neuronal cell model of neuroblastoma SH-SY5Y cells expressing fluorescently labeled FL-Tau1N4R (P301S) aggregates was used to investigate whether FL-Tau aggregates could affect autophagic flux and activity, to monitor their half-life and to understand if they are degraded by autophagy.

My findings suggested that FL-Tau aggregates seemed not to impair autophagic flux nor activity and that they were likely to be recognized by autophagic receptors, but their clearance was not efficient. Additionally, my results highlighted the importance to develop a reliable model to clarify the controversial relationship between Tau aggregates and autophagic defects in tauopathies.

2. INTRODUCTION

2. 1 Tauopathies and Tau protein

Tauopathies are a class of neurodegenerative diseases (NDs) all characterized by aberrant assembly of Tau protein into insoluble aggregates, accompanied by synaptic dysfunction and neural cell death (Guo et al., 2017). Characteristic signs and symptoms of these pathologies include movement disorders, cognitive decline, and dementia (Peller, et al., 2009). Among tauopathies, Alzheimer's disease (AD) is by far the most common one. Whereas AD is also characterized by the presence of extracellular amyloid-beta deposits (senile plaques), other tauopathies such as Progressive Supranuclear Palsy (PSP), Corticobasal Degeneration (CBD), Pick's disease (PiD) and Primary age-related tauopathy (PART) are primarily characterized by presence of Tau pathology (Vogels et al, 2019).

Tau is a microtubule-binding protein encoded by the "Microtubule associated protein Tau" (*MAPT*) gene, located on chromosome 17q21. In the human adult brain, alternative splicing of exons 2, 3 and 10 on MAPT gene generates six different isoforms which range from 352 to 441 amino acids. These isoforms differ by the presence of zero, one or two acidic N-terminal domains (0N, 1N, or 2N), and by the presence of three or four repeats (3R or 4R) in the microtubule-binding domain (MTBD), referred to also as repeated domain (RD) (**Fig. 1A**). Tau's RD represents the assembly-competent core of Tau filaments, as it has high propensity to generate β-structure (Guo et al., 2017).

In healthy neurons, Tau binds to microtubules and it is constantly phosphorylated and dephosphorylated to regulate microtubules assembly and stability, which are critical for axonal outgrowth and transport of cellular components along the microtubules (Jiang and Bhaskar, 2020). In pathological states, like AD, Tau becomes hyperphosphorylated and detaches from microtubules, leading to their destabilization and disassembly (Jiang and Bhaskar, 2020). Upon detachment from microtubules, Tau can exist as monomeric soluble form or can generate oligomeric Tau assemblies, which can interact to form paired-helical filaments (PHFs) that eventually grow into insoluble neurofibrillary tangles (NFTs) (Jiang and Bhaskar, 2020) (**Fig. 1B**).

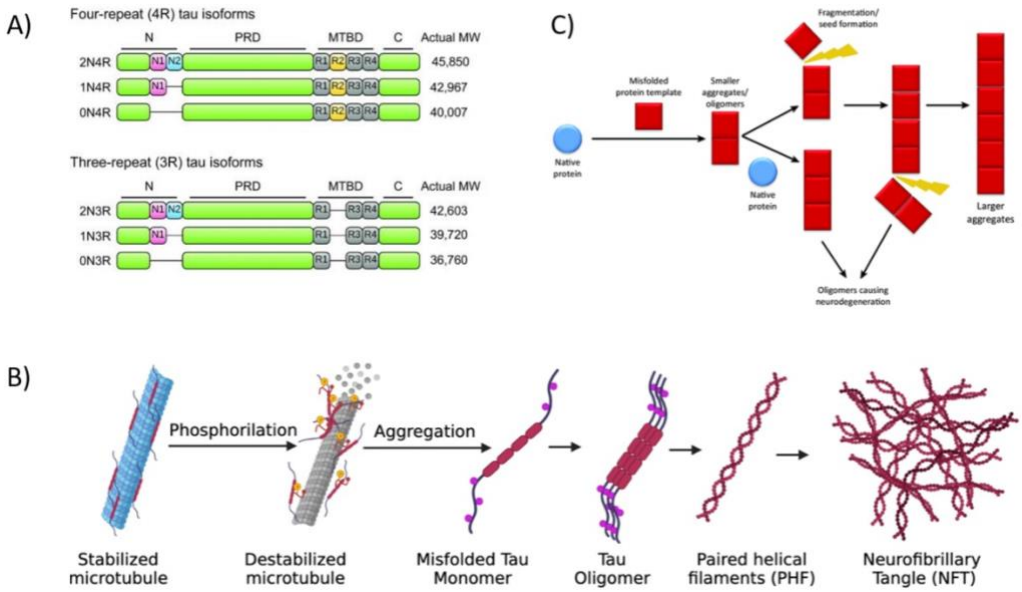

Figure 1. Tau structure and formation of insoluble aggregates. A) In the human brain, alternative splicing of the MAPT gene generates six Tau isoforms with different molecular weight (MW) (Guo et al., 2017). **B)** Hyperphosphorylated misfolded Tau detaches from microtubules and form soluble oligomers, which eventually aggregate in Neurofibrillary tangles (NFTs) (image created with Biorender.com). **C)** Illustration of prion-like propagation of pathological aggregates (image adapted from Silva et al., 2014).

Large numbers of NFTs are diagnostic markers for AD, albeit less numbers of these lesions have been shown to contribute to memory loss also in normal aging and in mild cognitive impairment (MCI) (Guillozet et al., 2003). Several hypotheses have been proposed to explain how AD evolves. The progression of the disease can be associated with NFTs' propagation in a prion-like manner, meaning that they can act as templates to induce the conversion of a native protein into a fibrillary form, thus leading to formation of new aggregates (Blaudin de Thé et al., 2021) (**Fig. 1C**). Moreover, disease advance is also linked to NFTs spreading through patients' brain. NFTs start to arise at least one decade before the appearance of the symptoms and during this time they spread following a well-defined pathway: from the enthorinal cortex to limbic region, including the hippocampus region, to ultimately reach the neocortex, which is invariably associated with cognitive symptoms (Braak H and Braak E, 1981; Braak et al., 2011; Holtzman et al., 2011). To date, due to the lack of suitable models, molecular mechanisms of Tau aggregation and accumulation are not yet completely understood (Lim et al., 2014).

2.2 Clearance mechanisms of Tau protein

One factor that could contribute to the spread and the accumulation of aggregates in tauopathies is the defective intracellular clearance by the ubiquitin proteasome system (UPS) and/or the autophagic system (Blaudin de Thé et al., 2021).

In healthy neurons, misfolded soluble Tau is degraded in an ATP- and ubiquitin-independent manner by the 20S proteasome system (**Fig. 2A**). However, pathologically modified Tau in AD is not degraded by the 20S proteasome due to its altered conformation. In this case, Tau may be polyubiquitylated with K48 linkages and turned over by the 26S proteasome (**Fig. 2B**) (Takashima et al., 2019). Nevertheless, polyubiquitinated Tau aggregates are likely not to be cleared by 26S proteasome, but instead they can impair it, thus generating aberrations in the UPS (**Fig. 2C**) (Takashima et al., 2019).

Several studies have proved that another major contributor of Tau removal is autophagy, the degradation system that allows clearance of intracellular components (damaged organelles and proteins, protein aggregates, pathogens, and nucleic acids) by lysosomes. Degraded material is then transported back to the cytosol and reused for different cellular purposes (Jiang and Bhaskar, 2020; Nakatogawa, 2020).

In healthy neurons, protein turnover of soluble wildtype is mediated by a specific form of autophagy, named endosomal microautophagy (e-MI). Generally, in microautophagy degradation cargo is directly internalized by lysosomal invaginations formed at the lysosomal membrane. Particularly, in e-MI the heat shock cognate 70 kDa (Hsc70) chaperone sequesters single soluble protein containing the KFERQ-like motif and delivers it to late endosomes, which can form membrane invaginations where the protein cargo is degraded (**Fig. 2D, panel A**) (Jiang and Bhaskar, 2020).

Soluble unmodified wild type Tau is shown to be degraded also by chaperone-mediated autophagy (CMA), where Hsc70 protein chaperone recognizes single soluble protein with a specific KFERQ-like motif (Wang et al., 2009). The chaperon-substrate complex then binds the cytosolic tail of lysosome-associated membrane protein type 2A (LAMP-2A), inducing its assembly in a multimeric complex which unfolds the protein and translocates it inside the lysosomal matrix

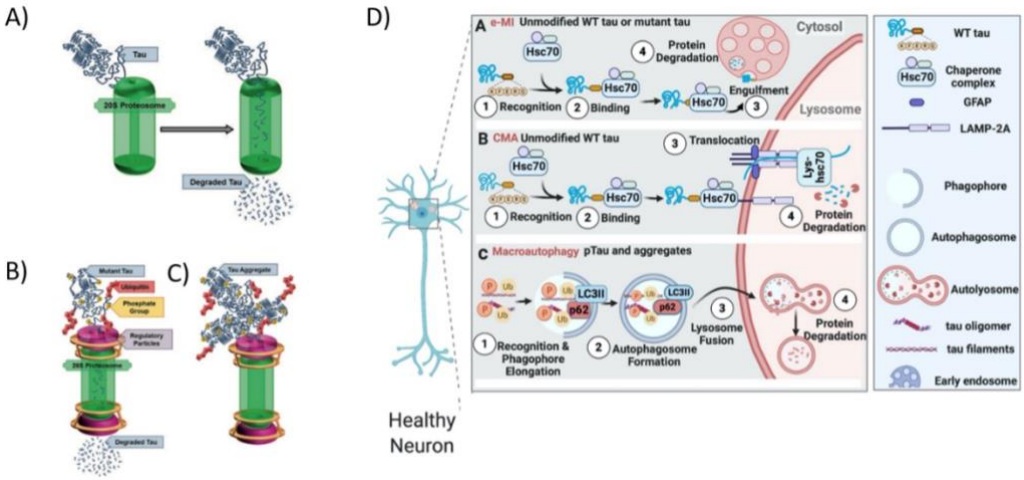

Figure 2. Tau clearance mechanisms. **A)** Tau is degraded by the 20S proteasome in an ATP- and ubiquitin-independent manner (image adapted from Takashima et al., 2019). **B)** Mutant Tau is ubiquitylated and degraded by the 26S proteasome (image from Takashima et al., 2019). **C)** Aggregated Tau is ubiquitylated but not degraded by the 26S proteasome (Takashima et al., 2019)**. D)** Panel A: WT Tau is degraded by e-MI. Panel B: WT Tau is degraded by CMA. Panel C: Tau aggregates are degraded by macroautophagy (image adapted from Jiang and Bhaskar, 2020).

for its degradation (**Fig. 2D, panel B**). However, the factors that determine Hsc70 sorting between CMA and e-Mi remain unknown (Jiang and Bhaskar, 2020).

Finally, soluble mutant Tau, such as the one harboring the aggregation-promoting ΔK280 mutation ($Tau_{RD}\Delta K$), was demonstrated to be degraded by macroautophagy, implying that it is engulfed by a membrane, that elongates and seals to form a double membrane vesicle, called autophagosomes. This latter fuses with lysosome for complete cargo degradation operated by hydrolytic enzymes (Wang et al., 2009; Jiang and Bhaskar, 2020) (**Fig. 2D, panel C**).

Concerning insoluble aggregates, previous studies proposed macroautophagy as the primary route for Tau aggregates degradation (Tan et al., 2008; Wang et al., 2009). However, there is still a debate on which pathway could primarily contribute to removal of the abnormal Tau aggregates (Wang et al., 2009).

2.3 The core autophagic machinery in macroautophagy

Specifically, degradation of protein aggregates by macroautophagy is named aggrephagy. Nutrient starvation, hypoxia, DNA damage, microbial infection, and

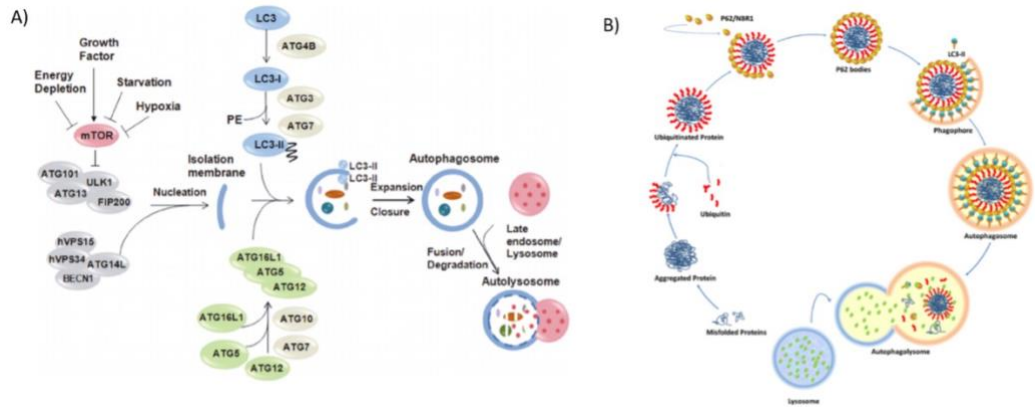

Figure 3. Autophagic machinery and key steps of aggrephagy in mammals. A) Inhibition of mTORC1 complex leads to activation of ULK1 at the phagophore formation site. ULK1 in turn recruits the PI3K complex, which generates PI3P on the isolation membrane (IM) to synthesize LC3-II. LC3-II is essential for IM elongation, maturation into autophagosome and fusion with lysosome for generation of autolysosome where cytoplasmatic cargo is degraded (image from Karakaş and Gözüaçik, 2013). **B)** Lys-63 ubiquitinated protein aggregates are recognized by autophagic receptors (such as p62) which by binding LC3, bridge protein aggregates to autophagosome membrane for their degradation (image adapted from Ma et al., 2019).

presence of damaged organelles, can all induce macroautophagy (Nakatogawa, 2020).

These signals inhibit mammalian target of rapamycin complex 1 (mTORC1), allowing autophagy activation for stress adaptation and cell survival (**Fig. 3A**). mTORC1 regulates autophagy in a transcription-independent manner. In presence of nutrients, mTORC1 is active and through phosphorylation inhibits complexes involved into autophagy initiation, such as ULK1 kinase complex. Under starvation, mTORC1 is inactivated and dissociates from ULK1, freeing it to trigger autophagosome formation (Nakatogawa, 2020).

The mammalian ULK1 consists of four subunits: ATG13, FIP200, ATG101 and ULK1/ULK2. To induce autophagosomes formation, multiples copies of ULK1 complex are assembled and recruited to the ER, supported by the interaction of FIP200 with ER transmembrane proteins (VAPA/VAPB). At the ER membrane, ULK1 promotes the recruitment of ATG9-containing vesicles which function as an initial membrane source for the autophagosome precursor (also named phagophore or isolation membrane, IM) (Nakatogawa, 2020). At the phagophore formation site

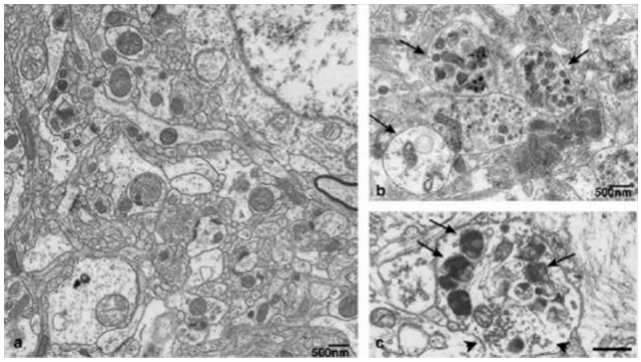

Figure 4. Autophagic defects in AD brains' patients. Autophagic vesicles (Avs) are normally rare in brain (a) but common in neuronal dendrites (b) and synaptic terminals (c) in AD (image from Nixon et al., 2005).

(PAS), ULK1 complex subunits ATG13 and ATG101 also recruit the PI3K-3 complex (consisting of VPS34, Beclin1, p150 and Atg14L), which enriches the phagophore with phosphatidylinositol-3-phosphates (PI3Ps) (Nakatogawa, 2020). PI3Ps is recognized by WIPI2b protein bound to ATG16L, which mediates the lipidation of ATG8-family proteins (microtubule associated protein light chain (LC3) isoforms) on the phagophore (Nakatogawa, 2020).

Initially, ATG4 proteases cleave LC3 isoforms to form the cleaved-LC3 (LC3I). Then, ATG7 (E1 enzyme) and ATG3 (E2 enzyme) cooperate with ATG16L (E3 enzyme) to conjugate the phosphatidylethanolamine (PE) to the cleaved LC3, thus forming LC3-PE (or LC3II) (Nakatogawa, 2020). LC3-II exerts different functions including cargo recruitment, fusion with lysosomes and phagophore maturation by recruitment of ATG2/WIPI complex. This latter promotes phagophore expansion by favoring lipid transfer from ER to phagophore. Although ER is the most promising candidate for lipids sources, they can also come from mitochondria, PM, Golgi, and *de novo* synthesis (Nakatogawa, 2020).

Once the phagophore has expanded, autophagosome formation is achieved by the closure of the pore, mediated by the ESCRT complex. The fully formed autophagosome then fuses with lysosomes and become autolysosome, where the hydrolytic enzymes (proteases, lipases, nucleases, and glycosidases) degrade the cargo. Lysosomal permeases release the breakdown products (amino acids, lipids, nucleosides, and carbohydrates) into the cytosol, where they are available for synthetic and metabolic pathways (Nakatogawa, 2020).

In aggrephagy (**Fig. 3B**), selectivity is ensured by autophagic receptors which recognize ubiquitinated protein aggregates. Firstly, E3-ligases mediate Lys-

63 polyubiquitination of aggregates which are then recognized by autophagic receptors through their Ub-binding motifs (Ma et al., 2019). p62/SQSTM1 receptor plays a crucial role in aggrephagy as it forms p62-bodies through self-polymerization and recruit further receptors, such as NBR1 and TAX1BP1. This receptor complex interacts with ULK1 complex subunit FIP200, for recruitment of the downstream autophagic machinery and formation of autophagosomes around p62 bodies. In addition, autophagic receptors harbor LC3 interacting regions (LIR), which mediate their interaction with LC3 proteins to promote cargo tethering on phagophore membranes (Simonsen and Wollert, 2022). Besides p62, NBR1 and TAX1BP1, other known aggrephagy receptors are OPTN (optineurin) and TOLLIP, which also bridge LC3 family members with ubiquitinated substrates (Chen et al., 2021). Upon autophagosome fusion with lysosome, autophagic receptors and LC3-II are degraded together with protein cargo inside the autolysosome (Simonsen and Wollert, 2022).

In AD patients, NFTs, which mainly consist of hyperphosphorylated Tau, are also positive for p62 receptors and ubiquitin (Li et al., 2022). Precisely, it was shown that in AD NFTs could receive linear ubiquitination and PHFs could undergo K63-polyubiquitination, suggesting that these pathological structures could be introduced to proteolysis through autophagic pathway (Nakayama et al., 2019; Li et al., 2022). However, a striking accumulation of autophagic vacuoles, such as autophagosomes and autolysosomes, was seen in neuronal dendrites and synaptic terminals of AD patients, suggesting impairment of autophagy in AD (Nixon et al., 2005) (**Fig. 4**). Nevertheless, it is still unclear whether Tau aggregates are causing autophagic defects or if their accumulation is due to dysfunction of autophagic system (Silva et al., 2020).

2.4 Understanding the relationship between FL-Tau aggregates and autophagy

The relationship between Tau aggregates and autophagy was already investigated by two members of the lab, Patricia Chastagner and Christel Brou. They created a human neuronal model of neuroblastoma SH-SY5Y cells stably expressing YFP-tagged RD-Tau via lentiviral transduction (Chastagner et al., 2020). Upon internalization of exogenous Tau fibrils containing the RD domain (K18 fibrils),

endogenous RD-YFP Tau was transformed into RD-Tau aggregates. They showed that endogenous RD-Tau aggregates colocalize with p62 receptors and partially with Ub K63, but not with autophagosome marker LC3 nor with lysosomal marker LAMP1 upon autophagic inhibition with Bafilomycin A1 (a drug that blocks fusion of autophagosomes with lysosome) (Chastagner et al., 2020). Hence, their results suggested that endogenous RD-YFP aggregates can be recognized as autophagic cargo, but they are likely to escape autophagic degradation. However, they did not have any proof that Full-length (FL) Tau aggregates would have the same fate inside the cells.

Therefore, during my internship, I used neuronal cell model stably expressing fluorescently labelled FL-Tau aggregates to investigate whether they can affect autophagic flux. This was done by performing western blotting and confocal analysis to monitor levels of autophagic receptors and LC3-autophagosome marker.

The second aim of my internship was to understand whether FL-Tau aggregates escape autophagic clearance. To assess this point, I first checked aggregates stability over time by extracting insoluble cellular components and monitoring FL-Tau aggregates presence by western blotting. Then, I conducted immunofluorescence analysis to see whether FL-Tau aggregates colocalize with autophagic receptors, autophagosomes and lysosomes.

3. MATERIAL AND METHODS

3.1 Cell culturing

For this study, SH-SY5Y cell line originated from human bone marrow with neuroblastoma was used (here referred as SH-WT). For GFP-SH, SH-SY5Y cells were transformed by lentiviral transduction. For C5 cells, SH-SY5Y cells were infected with a lentivirus expressing FL Tau1N4R (P301S)-mclover3 under the control of a Tet-off promoter. Next, a clonal population was obtained by limiting dilution. For H9A10 cells, C5 clones were treated with K18-ATTO594 fibrils to induce conversion of soluble FL-Tau into FL-Tau insoluble aggregates. Treatment with Doxycyclin was done for three days to repress FL-Tau transcription, before sorting clover-positive cells. To have a clonal population of cells expressing aggregates, 2 additional steps of limiting dilutions were performed.

For this work, all SH-SY5Y cells were grown in 25 cm^2 or 75 cm^2 flasks (Thermo scientific) and maintained in RPMI-1640 (Euroclone), 10% Fetal Bovine Serum (FBS) and 1% Penicillin/Streptomycin (P/S). At time of harvest, cell media was removed from the flasks and cells were rinsed with Dulbecco's Phosphate Buffer Saline without CaCl2 and MgCl2 (PBS -/-) (Gibco). Appropriate amount of pre-warmed 0.05% Trypsin-EDTA (Gibco) was added, and flasks were incubated for 2-3 min at 37°C until cells were lifted from the plate. Finally, pre-warmed serum-containing medium was added to inactivate trypsin.

3.2 Protein extraction and quantification

SH-WT, SH-GFP, C5 and H9A10 cells were counted using a Bio-Rad TC10™ Automated cell counter. 10^6 cells were plated onto 60 mm plates (Falcon® Cell culture Dish) and kept at 37°C, 5% CO_2, O/N. The next day, cells were treated with DMSO or Bafilomycin (320 nM, Sigma) in complete or serum free medium for 3H. Cells were scraped and resuspended in Dulbecco's Phosphate Buffer Saline with $CaCl_2$ and $MgCl_2$ (PBS +/+). After centrifugation at 2000 rpm for 3 min at RT, the supernatant was discarded and cell pellets were lysed with lysis buffer (Nacl 300 mM, Triton 1%, MgCl2 5mM, Tris 50 mM pH 7.4) containing 1X Protease inhibitor (Roche). Lysates were kept on ice for 30 min and then centrifuged at 14.000g, for 30 min, at 4°C. The cytosolic fraction was collected, and proteins quantified with

the Bradford method. 2.5 ul of each extract was added to a cuvette with 1ml Quick Start™ Bradford 1X Dye reagent and measured by a spectrophotometer at 595nm. Using a protein standard curve, the absorbance value calculated against a blank control was used to calculate the protein concentration.

3.3 Extraction of soluble and insoluble proteins

For extraction of soluble and insoluble material, untreated and Dox-treated (30 ng/ml, Sigma) C5 and H9A10 cells were grown in a 75cm^2 flasks and incubated O/N at 37 °C. The next day, trypsinized cells were counted and 10^6 cells were centrifuged at 1500 rpm for 5 min at RT. The supernatant was discarded, and cell pellets were stored at -20 °C. Frozen cell pellets were thawed on ice and resuspended in PBS +/+ containing 0.05% Triton-X. The lysates were centrifuged at 500g for 5 min at RT to discard the nuclei pellet. The non-nuclei supernatant was centrifuged again at 1000g for 5 min at RT. The supernatant was collected and ultracentrifuged at 100.000g for 1 hour at 4°C. The product supernatant was collected as soluble fraction. The pellets were washed in PBS +/+ and resuspended in RIPA buffer (25mM Tris pH 7.4, 150 mM NaCl, 0.5 % Sodium deoxycholate, 1% Triton) with 2% SDS and 25mM DTT. Protein quantification was done only for the soluble fraction, by adding 10 ul of soluble extracts in 1ml Quick Start™ Bradford 1X Dye. This was not done for the insoluble one as the RIPA detergents affect the Bradford dye reaction.

3.4 Gel electrophoresis and Western blot

For gel electrophoresis, 10 or 50 ug of protein extracts were used. The insoluble fraction was loaded according to the volumes of the corresponding soluble fraction. Samples were mixed with water and 1xLaemmli (Bio-rad) containing DTT. All samples were boiled for 3 min at 100 °C and loaded on a Criterion™ XT Precast Gel 4-12% Bis-Tris (Bio-Rad) or on a NuPAGE™ 4-12 % Bis-Tris gel (Thermo Scientific). The run was done in 1x MES buffer (Bio-Rad) or in 1xMOPS (Bio-Rad), initially at 80 V and then at 100 V until proteins reached the bottom. Total protein samples were transferred on a PVDF membrane (Amersham Hybond P 0.45), previously soaked in 100% ethanol, and rehydrated in water. Transfer was done using 1x Transfer Buffer (Tris-Base 0.005M, Glycine 0.0384M) at 100 V for

45 min at 4 °C. Membranes were blocked in 5% non-fat milk in 1x Tris- Buffered Saline with 0.1%Tween (TBST) for 1 hour at RT. For protein detection, membranes were incubated with primary antibodies **(Table 1)** diluted in 5% non-fat milk in TBST. For anti-p62, anti-LC3 and anti-GFP incubation was performed O/N at 4 °C; for anti-GAPDH it was done for 1.5 hour at RT. Membranes were washed 3 times for 10 minutes each with TBST and incubated with secondary HRP-conjugated antibodies **(Table 1)** diluted in 0.5% non-fat milk in TBST for 45 minutes at RT. Membranes were washed 3 times for 10 min each in TBST before adding ECL plus western blot substrate (Thermo scientific). Images were acquired by using Amersham image 680 and raw data (non-saturated images) analyzed with ImageJ.

3.5 Immunofluorescence

For immunofluorescence 50K of all SH-SY5Y cells were cultured in µ-Slide 8-Well plates (Ibidi) the day before the experiment. After O/N incubation at 37 °C, cells were untreated or treated with Bafilomycin (320 nM, Sigma) for 3 hours. The medium was discarded, and cells were fixed with 2% PFA for 20 min at RT. Fixation was followed by treatment with NH_4Cl for 10 min at RT and one wash in PBS +/+. Cells were left O/N at 4°C and the next day permeabilized with PBS +/+ containing 10% FBS, 0.05% Saponin for 5 min at RT. Cells were then incubated with primary antibodies **(Table 1)** diluted in PBS +/+ 10% FBS, 0.05% Saponin for 1.30 hour. After 3 washing steps in PBS +/+ 10% FBS, 0.05% Saponin, cells were incubated with the secondary antibody **(Table 1)** diluted in PBS +/+ 10% FBS, 0.05% Saponin for 45 min, in dark condition. After 3 washing steps with PBS +/+ 10% FBS, 0.05% Saponin and 2 with PBS +/+, cells were stained for 1x Hoechst diluted in PBS +/+ for 5 min. Finally, cells were washed 3 times in PBS +/+ and stored at 4°C. Image acquisition was performed by using Zeiss LMS 700 Inverted Microscope. Images were analysed using Icy software.

Table 1. List of antibodies used for Immunoblot and Immunofluorescence analysis.

	Name	Origin	WB	IF	Producer	Reference
Primary antibodies	Anti-LC3	Rabbit	1:1000	1:400	Sigma	L7543
	Anti-p62	Mouse	1:1000		Abnova	H00008878-M01
	Anti-GAPDH	Mouse	1:5000		Sigma	G9545
	Anti-GFP	Rabbit	1:500		Life Technologies	A-6455
	Anti-p62	Guinea pig		1:500	Progen	GP62-C
	Anti-Tax1BP1	Rabbit		1:50	Sigma	HPA024432
	Anti-Lamp1	Mouse		1:400	DSHB	1D4B
Secondary antibodies	Anti-Rabbit-HRP	Donkey	1:10000		Cytiva	NA934V
	Anti-Mouse-HRP	Sheep	1:10000		Cytiva	NXA931V
	Alexa Fluor™ 488 Goat anti-rabbit	Goat		1:1000	Invitrogen	A11034
	Alexa Fluor™ 546 goat anti mouse	Goat		1:1000	Invitrogen	A11030
	Red cy3 goat anti-guinea pig	Goat		1:1000	Bethyl Laboratories®	BE-A60-210C3
	Alexa Fluor™ 546 goat anti rabbit	Goat		1:1000	Invitrogen	A11035

4. RESULTS

4.1 Investigation of FL-Tau aggregates effects on autophagic flux

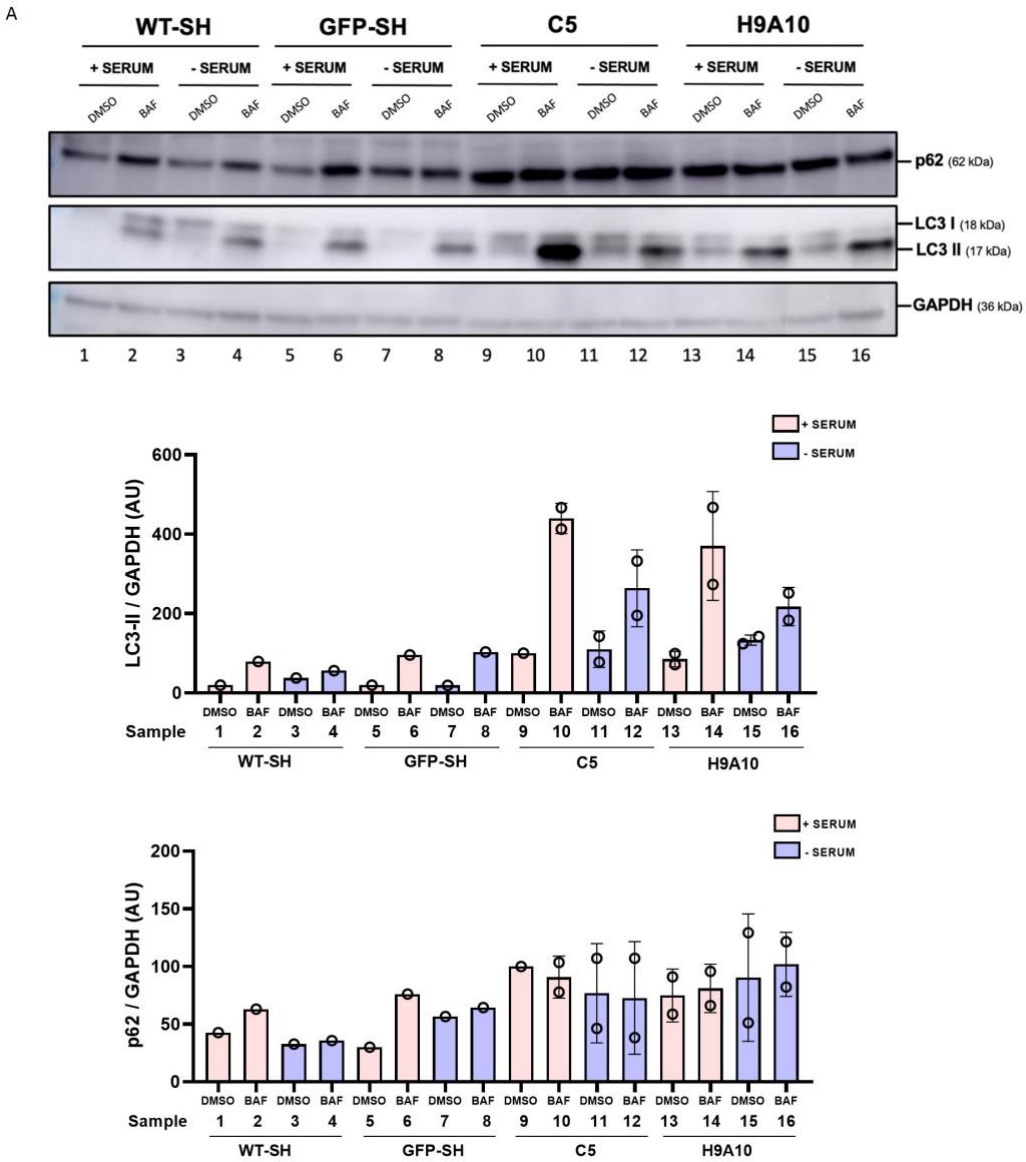

Figure 5. Investigation of FL-Tau aggregates effects on autophagic flux. A) WT-SH, GFP-SH, C5 and H9A10 cell lines were grown for 3H in presence and in absence of serum. Cells were treated with Baf (320 nM) for 3H, concomitantly to starvation. After treatment, cells were harvested and protein extracts were quantified using Bradford protein assay. 50 ug of each protein extract was run on a 4-12% Bis-Tris gel in MES buffer (denaturation in 1X Laemmli with DTT) and transferred on a PVDF membrane. Protein were detected by primary antibodies p62-Mouse (Abnova, 1:1000), LC3B-Rabbit (Sigma, 1:1000), GAPDH-Rabbit (Sigma, 1:5000). Representative image for 1 experiment for WT-SH and GFP-SH, for 2 independent experiments for C5 and H9A10 cells. Graphs showing protein levels normalized to GAPDH and adjusted to C5 untreated sample in optimal conditions are presented in AU. Standard deviation was used for the error bars.

To investigate whether the presence of overexpressed FL-Tau-mclover3, under its soluble or aggregated form, affects the autophagic flux I performed immunoblot analysis to monitor LC3-II and p62 levels in C5 cells and H9A10 cells. C5 cells derive from SH-SY5Y cells infected with a lentivirus expressing the P301S-FL-Tau (1N4R) mutant, which has higher propensity to aggregate into abnormal filaments (Chastagner et al., 2020). Besides, FL-Tau was coupled with the green fluorescent protein mclover3. H9A10 cells derived from C5 clones treated with K18 fibrils to convert soluble FL-Tau into FL-aggregates. Wild type cells (WT-SH) and cells overexpressing GFP (GFP-SH) were taken as control for the comparisons with C5 and H9A10.

Prior to immunoblot analysis, cells were grown for 3 hours in optimal condition or in serum starvation, which is expected to induce autophagy by inhibition of mTORC1 complex (Zhang et al., 2016). Next, cells were lysed, and protein extracts were separated on a gel and transferred on a PVDF membrane, which was incubated with LC3 and p62 primary antibodies. Finally, protein expression was quantified relative to GAPDH used as loading control.

Since both LC3-II and p62 are degraded during autophagy, protein levels were quantified both in absence and in presence of BafilomycinA1 (Baf), a drug that impairs lysosomal function and prevents autophagosome-lysosome fusion (Zhang et al., 2016). In this experiment, Baf treatment was performed for 3 hours, concomitantly to serum starvation. To evaluate the level of autophagic flux, we considered the difference of LC3-II levels between Baf-treated samples and untreated samples, which represents the amount of autophagosomes that have been delivered and degraded by lysosomes (Zhang et al., 2016). To monitor autophagic activity we used LC3-II levels in presence of Baf, which correlate with the number of autophagosomes generated inside the cells (Zhang et al., 2016).

For WT-SH cells grown in optimal condition, immunoblotting of LC3-II (**Fig. 3A**) showed a difference of LC3-II levels in presence and absence of Baf (sample 2 - 1), suggesting presence of autophagic flux in accordance with these cells undergoing high level of autophagy (Klionsky et al., 2016). Similar results were observed in WT-SH cells under serum starvation (compare sample 4 - 3 to 2

- 1), conveying the impression that the short period of starvation is not enough to increase the flux nor to enhance autophagosome formation.

GFP-SH cells were used as control for C5 cells to monitor the effects of mclover3 overexpression. These cells did not show any remarkable difference with WT-SH cells, implying that overexpression of GFP was not perturbing autophagic flux nor autophagic activity in none of the investigated growth condition.

As well as WT-SH cells in optimal condition, also C5 and H9A10 cell lines showed presence of autophagic flux as proved by to the difference of LC3-II levels between Baf-treated and untreated samples (for C5, sample 10 - 9; for H9A10, sample 14 - 13). Autophagic flux was also noticed in serum-starved C5 (sample 12 - 11) and H9A10 cells (sample 16 - 15).

Nevertheless, in presence of the inhibitor both C5 and H9A10 cells showed noticeable increase of LC3-II compared to WT-SH (compare samples 10 and 14 to sample 2), indicating that likely there was an increase of autophagic activity.

To further investigate the effects of FL-Tau aggregates on autophagic flux, I performed visualization of LC3 puncta by fluorescent microscopy (**Fig. 7A**). For this experiment, cells were grown O/N in optimal condition and treated with Baf for 3H, which was expected to increase autophagosomes number (LC3 puncta) by blocking their fusion with lysosomes. Then, cells were fixed, permeabilized and treated with LC3 primary antibody. Also in this case, the flux was monitored by comparing the number of LC3 puncta in the presence and in absence of Baf. As expected, qualitative results from 3 independent experiments clearly showed that in all Baf-treated SH-cells number of LC3 puncta increased compared to untreated cells. Moreover, both in Baf-treated and untreated cells expressing soluble FL-Tau LC3-puncta were more compared to the control cells, in line with immunoblot showing increased LC3 levels in the same conditions. However, H9A10 cells did not show any striking differences compared to C5 cell neither in the difference of LC3 puncta between Baf-treated and untreated conditions, nor in the number of LC3 puncta in presence of the inhibitor.

Hence, both immunoblot and confocal analysis suggested that overexpressed soluble FL-Tau did not perturb autophagic flux, but it was likely to enhance autophagosomes formation. By contrast, compared to soluble FL-Tau,

insoluble FL-Tau aggregates seemed not to alter the flux nor to affect autophagic activity.

In addition to LC3-II, I monitored p62 levels a selective substrate of autophagy, whose levels inversely correlates with autophagic activity. Accumulation of p62 is a marker for autophagy suppression, while decreased levels indicate induction of autophagy (Zhang et al., 2016). As well as for LC3-II, p62 levels were measured in presence and in absence of Baf to determine the amount of protein substrate that is degraded.

In WT-SH cells grown in presence of nutrients there was a slight difference of p62 protein levels between Baf-treated and untreated samples (samples 2-1). This means that protein cargo is likely to be recruited and delivered to autophagosomes for lysosomal degradation. Again, wild type-starved cells (samples 4-3) were behaving similarly to WT-SH cells in optimal condition. This held also for GFP-SH cells, both in optimal and starvation condition, implying that neither 3H starvation nor overexpression of GFP are perturbing autophagic flux nor autophagic activity.

Different from SH-WT cells, in both the investigated growth conditions immunoblot of p62 in cells overexpressing soluble Fl-Tau showed higher levels of protein in presence of Baf (compare samples 10 and 14 to sample 2) and equal levels of p62 in Baf-treated and untreated samples (for C5 samples 10 - 9; for H9A10 samples 14 -13).

p62 levels were monitor also by confocal analysis (F**ig. 7A**). Results from 3 independent experiments showed that Baf treatment induced p62 stabilization in all SH-cells, resulting in puncta formation. Yet, different from immunoblot data, C5 and H9A10 cells did not showed equal levels of p62 between Baf-treated and untreated samples. However, p62 levels seemed to be higher in Baf-treated cells overexpressing FL-Tau compared to control cells.

Hence, although p62-immunoblot results created the impression of autophagy inhibition in cells overexpressing soluble Tau, p62 confocal visualization suggested presence of flux in all SH cells and enhancement of autophagic activity in cells with overexpressed soluble Tau. Nonetheless, when p62 levels were monitored in cells where expression of soluble FL-Tau was repressed by using Doxycycline, it was showed that the increase of p62 amount was not

correlated to soluble FL-Tau, thus suggesting that higher p62 levels were due to a clonal effect (**Fig 6 B-C**).

4.2 Monitoring FL-Tau aggregates half-life

Next, I wanted to determine whether FL-Tau aggregates are stable or degraded overtime and compare them to the soluble form. To address this point, I performed western blot of FL-Tau-mclover3 in C5 cells, which mainly contains soluble material, and H9A10, which mainly express FL-Tau in its aggregated form and less in its soluble one. In both cells, FL-Tau is under the control of a Tet-off promoter, meaning that addition of tetracycline-derivatives like doxycycline (Dox) turns off gene expression.

For this experiment (**Fig. 6A**), I daily treated cells with Dox for 7 days (D) and I collected samples from untreated cells and Dox-treated cells from D0, 1, 4, 5, 6 and 7 (this latter not shown). After cell lysis, samples were ultracentrifuged to separate the soluble material (S), which contains soluble FL-Tau-mclover3 monomers, from the insoluble material (I), where the insoluble FL-Tau aggregates are expected to be. Then, proteins extracts were separated on a polyacrylamide gel and transferred on a PVDF membrane which was treated with primary antibody GFP-rabbit to detect mclover3 portion of FL-Tau-mclover3. This latter is expected to have a molecular weight of approximately 75 kDa, as it comes from fusion of FL-Tau 1R4N (48 kDa) and mclover3 (27 kDa). Finally, for the soluble material I calculated the protein expression relative to GAPDH control (this was not possible for insoluble fraction).

For soluble FL-Tau-mclover3, constant protein levels in absence of Dox and decreasing levels in its presence were expected both in C5 and H910A. In C5 cells immunoblot results showed that, despite protein amount was changing over time and was quite far from predicted levels likely due to inaccurate experimental procedure, soluble FL-Tau-mclover3 seemed to be always expressed in absence of Dox. On the other hand, when Dox was added protein levels halved at D1 (estimated soluble protein Half-life from one experiment = ± 24H) and they kept diminishing over time (**Fig. 6B/C)**.

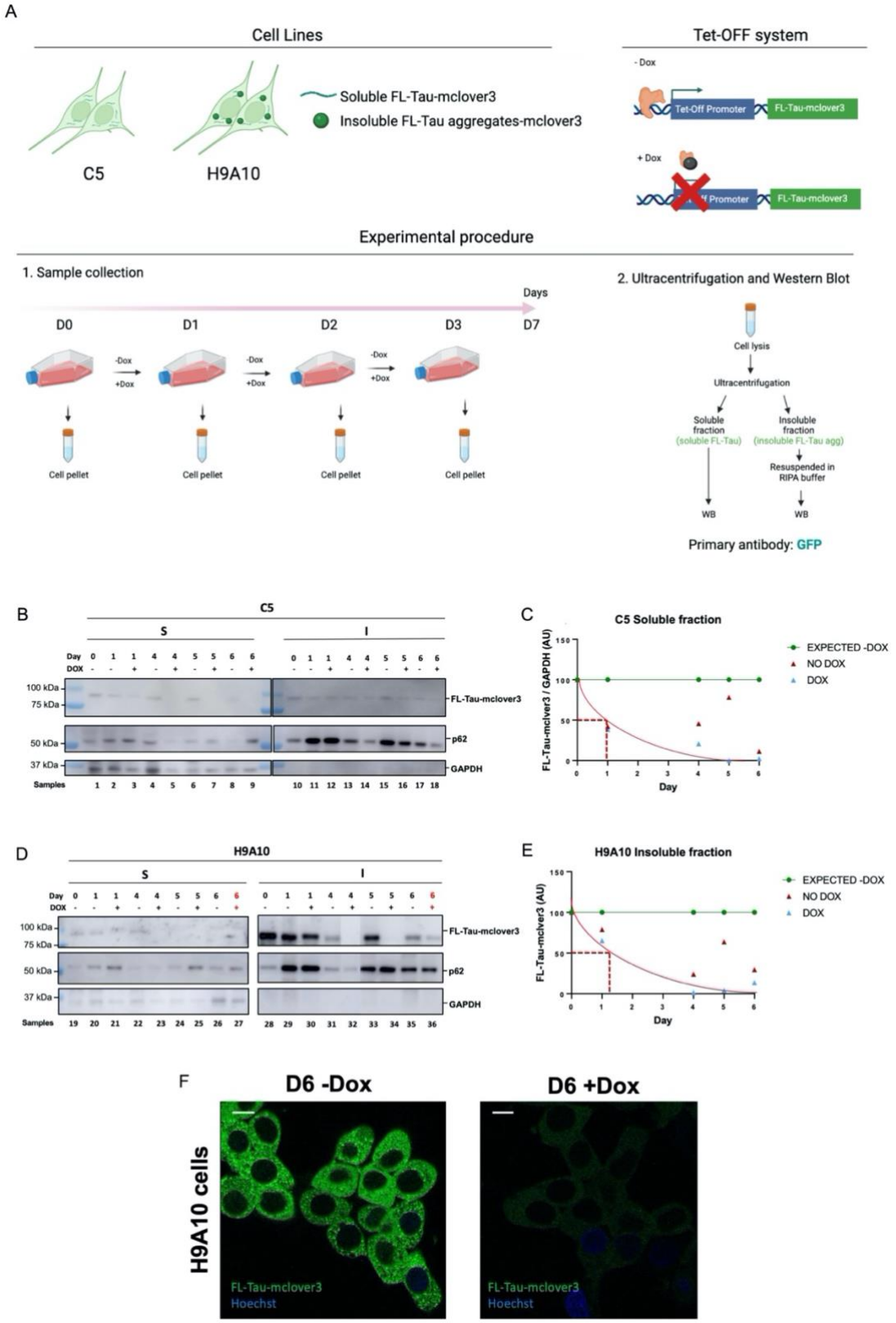

Figure 6. Monitoring FL-Tau aggregates half-life. A) Schematic rappresentation of used cell lines, TET-off system and experimental procedure. **B-E)** Untreated and Dox-treated C5 and H9A10 cells were lysed, and the soluble material was separated from the insoluble

one by ultracentrifugation. Soluble protein extracts were quantified by Bradford protein assay and 10 ug of each sample was added to loading solution. The insoluble fraction was resuspended in RIPA buffer and loaded according to the volume of corresponding soluble material. Proteins were run on a 4-12 % Bis-Tris gel (in 1x MOPS, denaturation in 1X Laemmli with DTT) and transferred on a PVDF membrane. Proteins were detected by primary antibodies GFP-rabbit (Life Technologies, 1:500), p62-mouse (Abnova, 1:1000) and GAPDH-Rabbit (Sigma, 1:5000). Protein bands were visualized using ECL plus western blotting substrate. Images were acquired by Amersham image 680. For H9A10 image, sample 32 was moved; see original membrane in **Supp. 1B**. Graphs showing expected protein half life and expression levels normalized to GAPDH and adjusted to D0 presented in AU. For H9A10 cells protein levels were not calculated relative to the control. Representative images for 1 experiment. S: Soluble. I:Insoluble. **F)** Confocal Images of untreated and Dox-treated H9A10 cells at D6. Cells were stained for Hoechst for 5 min. Scale bar: 10 um. Representative images for 1 experiment.

For H9A10 cells, levels of soluble FL-Tau-mclover3 were more difficult to detect compared to C5 cells, probably because in these cells FL-Tau-mclover3 is converted into aggregates soon after its expression (**Fig. 6D)**. However, since H9A10 cells derive from C5 cells, soluble FL-Tau was assumed to behave the same in the two cell lines and the protein half-life calculated for C5 should apply also for H9A10 cells.

Regarding the insoluble fraction, protein levels were not calculated relatively to the control, as this latter was absent in all the samples. Looking at the insoluble fraction of C5 cells (**Fig. 6B)**, all samples had similar levels of FL-Tau-mclover3, which might result from contamination of soluble fraction or from formation of spontaneous insoluble aggregates from overexpressed FL-Tau-mclover3.

For H9A10 cells insoluble fraction, detection of FL-Tau-mclover3 should indicate presence of FL-Tau aggregates. These latter were predicted to be stable in absence of Dox, where constitutive expression of soluble FL-Tau should ensure constant formation of new aggregates. Immunoblot results showed that in absence of Dox levels of insoluble materials were markedly higher compared to C5 cells, again due to straight aggregation of soluble protein into insoluble fibrils. Unexpectedly, aggregates were not stable overtime, and their amount was quite different from the theoretical one, likely due to imperfect experimental procedure. Nonetheless, aggregates were roughly always detected in untreated conditions. Looking at Dox-treated samples, aggregates levels started to diminish at D1 (sample 30; estimated

insoluble protein Half-life from one experiment = ± 24H), and they were absent at D4 (sample 32) and D5 (sample 34) (**Fig. 6D/E**). However, at D6 (sample 36) there was presence of insoluble material which might derive from sample D7 –Dox with which it was mixed, by assuming that aggregates should be stable over time.

All together, these results suggested that as expected Dox treatment impaired the production of de novo FL-Tau in both cells lines. Moreover, although in H9A10 cells accumulation of insoluble material suggested that FL-Tau is more stable in its aggregated conformation rather than in the soluble one, FL-Tau aggregates appeared to be likely degraded over time.

To further investigate the fate of FL-Tau aggregates, untreated and Dox-treated H9A10 cells at D6 were analyzed by confocal microscopy to monitor presence of aggregates. **Fig. 6F** shows that in Dox-treated cells there were less aggregates compared to the untreated sample, supporting the idea that FL-Tau aggregates were likely to be degraded.

Next, since p62 levels were previously shown to increase in cells expressing soluble FL-Tau-mclover3, I monitored the amount of p62 in untreated and Dox-treated C5 and H9A10 cells to see whether this higher expression was a clonal effect or was due to the presence of FL-Tau-mclover3. Immunoblot of p62 in C5 and H9A10 cells (**Fig. 6B-C**) showed that both in untreated and in Dox-treated samples soluble p62 is still detected at similar levels (for C5 compare samples 6 and 7; for H9A10 compare samples 24 and 25). The same holds for C5 and H9A10 insoluble fractions. Indeed, insoluble-p62 is still detected when corresponding soluble FL-Tau-mclover3 was downregulated (for C5 compare sample 15 and 16; for H9A10 compare samples 33 and 34).

Interestingly, insoluble-p62 levels were quite high in both cell lines, where previously I noticed increase of autophagic activity as demonstrated by higher levels of autophagosomes formation compared to control cells (**Fig. 5A**). This could explain the possible increase of p62 bodies as they were shown to act as platform for autophagosome formation (Kageyama et al., 2021).

Hence, these outcomes convey the impression that Dox is not affecting p62 soluble and insoluble levels and that FL-Tau-mclover3 is not responsible for the higher levels of p62 in the investigated cell lines.

4.3 Monitoring autophagic clearance of FL-Tau aggregates

Next, aiming to understand whether FL-Tau aggregates could potentially be degraded by autophagy, immunofluorescence (IF) analysis was performed to assess colocalization between FL-Tau aggregates, autophagic receptors (p62, TAX1BP1), autophagosomes (marked by LC3) and lysosomes (marked by LAMP1). WT-SH, GFP-SH and C5 cells were taken as control for H9A10 cells.

For this experiment, all SH-cells were grown O/N in optimal condition and the next day they were either left untreated or treated with Baf. Next, cells were fixed, permeabilized with saponin and treated with primary antibodies anti-p62, anti-TAX1BP1, anti-LC3 and anti-LAMP1.

Firstly, to see if FL-Tau aggregates were recognized as autophagic cargo and engulfed by autophagosomes I assessed their simultaneous colocalization with p62 and LC3 in Baf-treated and in untreated cells (**Fig. 7A**). In WT-SH and GFP-SH cells in absence of BAF, colocalization of p62 and LC3 was difficult to detect, likely due to their autophagic degradation. However, increment of p62 and LC3 puncta in response to Baf lead to a higher degree of colocalization, in line with cells undergoing autophagy. Compared to control cells, a mild increase of p62/LC3 colocalization was already seen in absence of Baf in both cell lines overexpressing FL-Tau and it was further reinforced by Baf. These observations confirmed my previous immunoblot data (**Fig. 5A**), which showed a potential enhancement of autophagic activity in cells overexpressing FL-Tau. Concerning H9A10 cells, qualitative observations from 3 independent experiments showed that very few FL-Tau aggregates were recognized by p62 and that most of them were not associated with p62 and LC3.

To further investigate recognition of FL-Tau aggregates as autophagic substrate, colocalization between FL-Tau aggregates and TAX1BP1 was assayed (**Fig. 7B**). Once more, in all SH-cells Baf led to receptor stabilization resulting in puncta formation, and the difference in TAX1BP1-puncta between Baf-treated and untreated cells confirmed presence autophagic flux. In cells expressing aggregates, a low degree of colocalization between TAX1BP1 and the aggregates was already appreciated in absence of Baf, and it did not remarkedly changed upon Baf addition. However, the majority of FL-Tau aggregated seemed not to colocalize with TAX1BP1.

Finally, to determine whether FL-Tau aggregates could have been delivered to lysosomes by autophagosomes, colocalization with LC3 and the lysosomal-associated membrane protein-1 (LAMP-1) was performed (**Fig. 7C**).

As presumed, all SH cells showed LC3 puncta increase in presence of Baf. Unexpectedly, Baf-treated WT-SH cells showed enlarged lysosomes. However, in the other three cells lines lysosomes dimension seemed not to be affected in presence of Baf. According to cells undergoing autophagy, colocalization between LC3 and LAMP1 was observed in all SH-cells, particularly in cells overexpressing FL-Tau. However, in H9A10 FL-Tau aggregates seemed not to colocalize neither with autophagosomes nor with lysosomes.

Furthermore, to investigate whether autophagy was involved into aggregates degradation, I observed the number of aggregates per cells under Baf-inhibitory treatment. However, results showed that aggregates remained stable in response to at least 3 hours of Baf-treatment (**Suppl. 1B).**

All in all, IF results confirmed my previous data showing that all SH-cells were undergoing autophagic flux and that autophagy seemed to be induced in cells overexpressing FL-Tau. Additionally, they suggested that FL-Tau aggregates were potentially recognized as autophagic cargo, but they were not associated with autophagosomes nor with lysosomes.

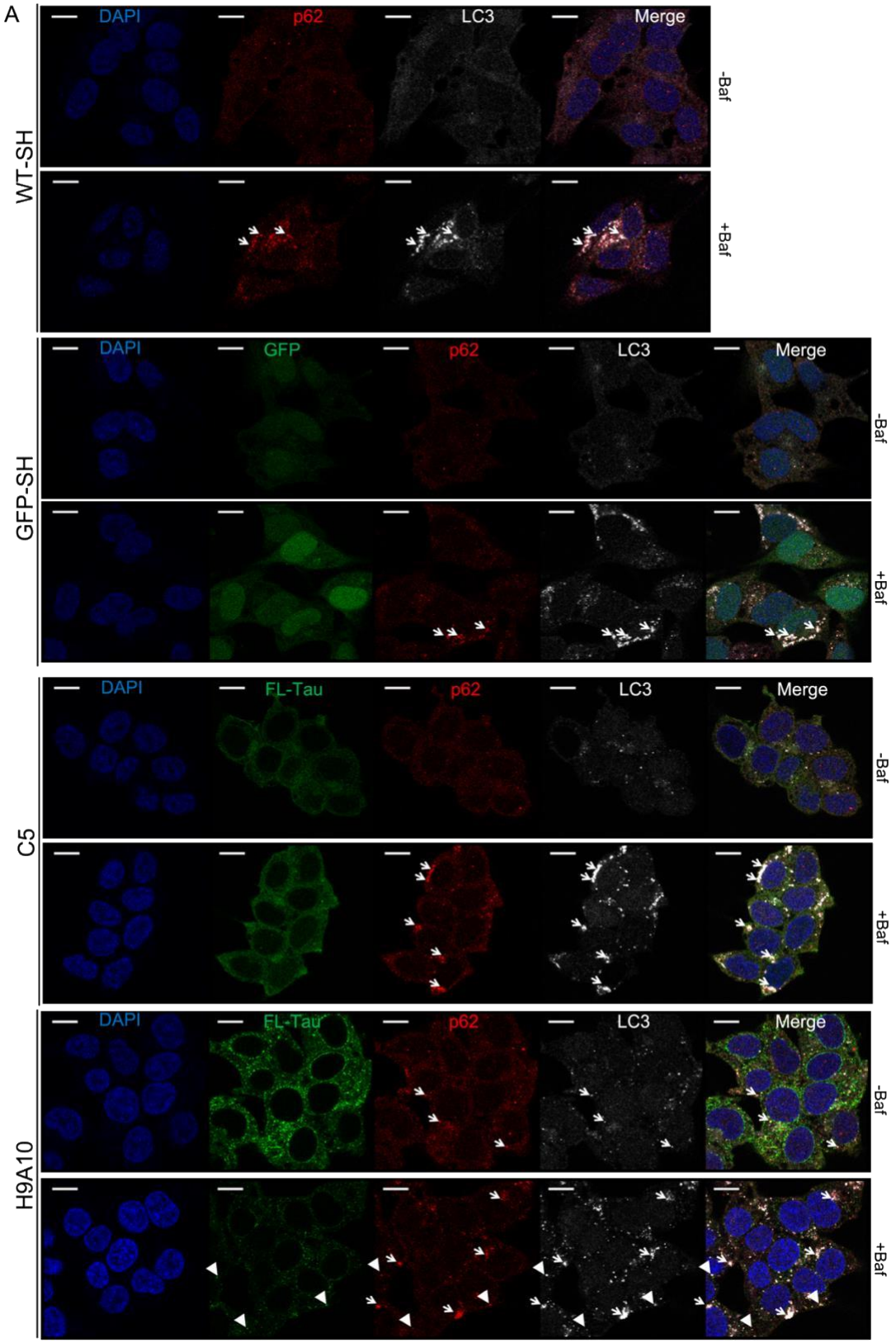
A
WT-SH
DAPI
p62
LC3
Merge
-Baf
+Baf
GFP-SH
DAPI
GFP
p62
LC3
Merge
-Baf
+Baf
C5
DAPI
FL-Tau
p62
LC3
Merge
-Baf
+Baf
H9A10
DAPI
FL-Tau
p62
LC3
Merge
-Baf
+Baf

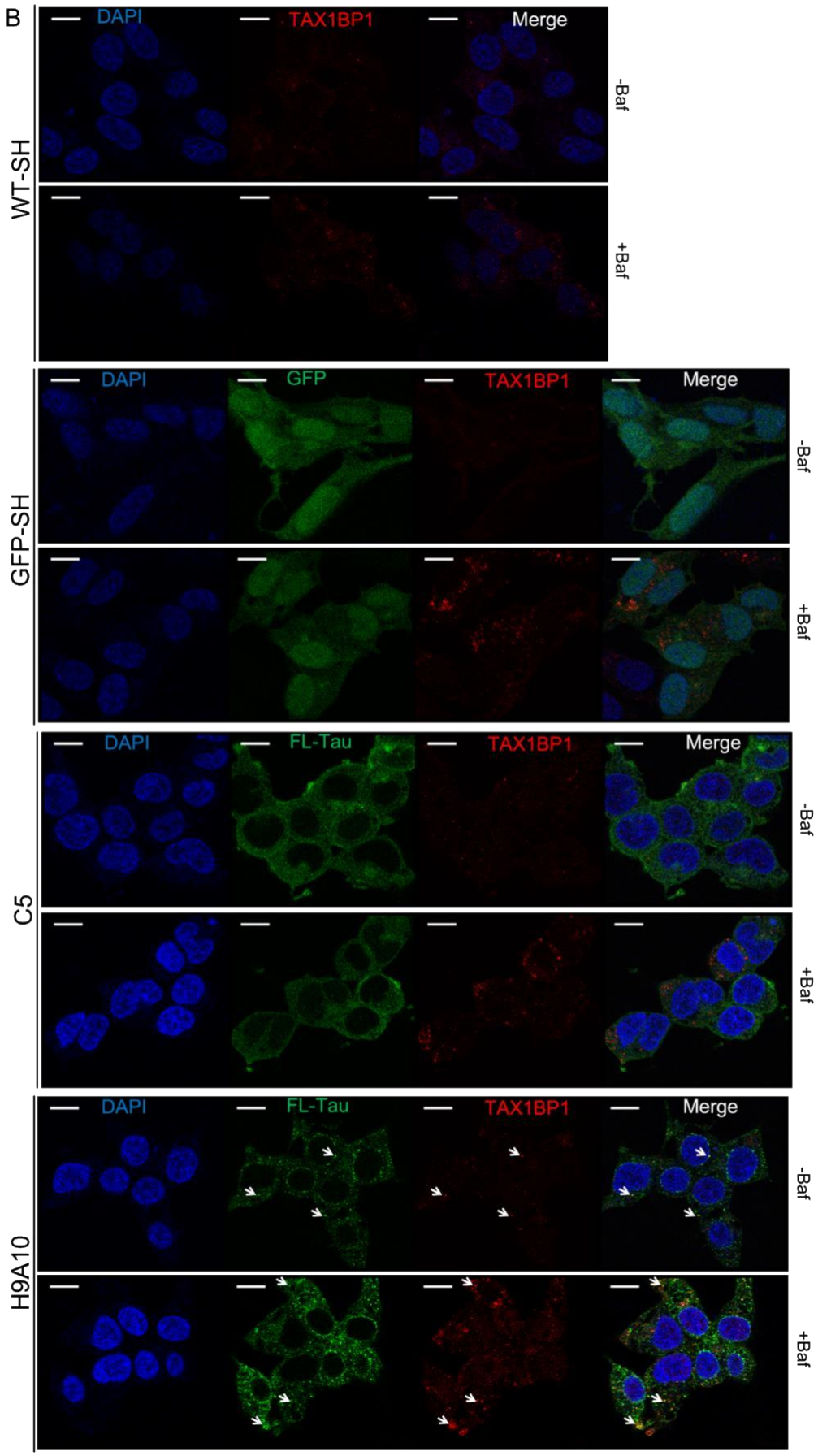
B
WT-SH
DAPI
TAX1BP1
Merge
-Baf
+Baf
GFP-SH
DAPI
GFP
TAX1BP1
Merge
-Baf
+Baf
C5
DAPI
FL-Tau
TAX1BP1
Merge
-Baf
+Baf
H9A10
DAPI
FL-Tau
TAX1BP1
Merge
-Baf
+Baf

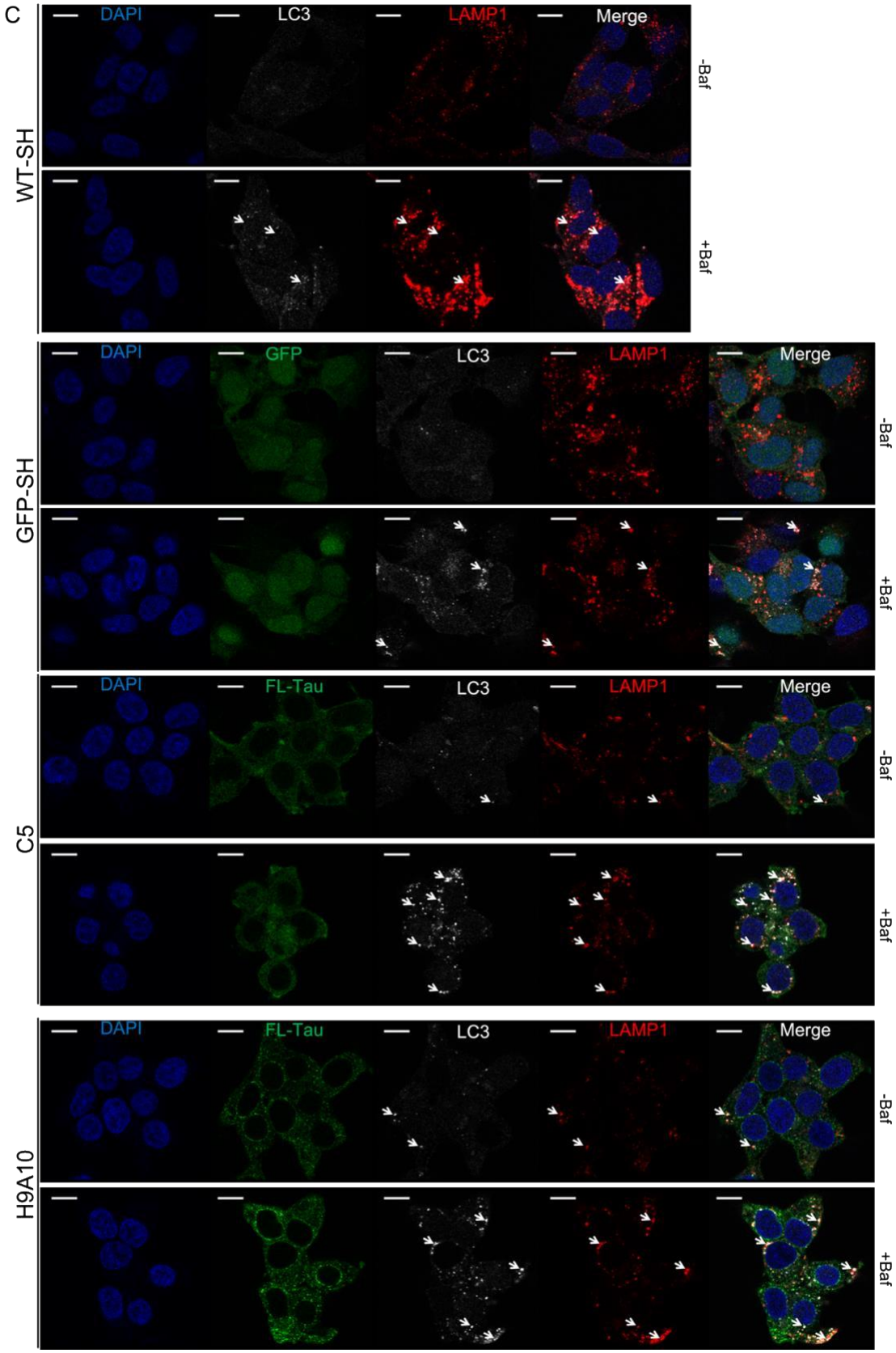
C
WT-SH
GFP-SH
C5
H9A10
DAPI
LC3
LAMP1
Merge
GFP
FL-Tau
-Baf
+Baf

Figure 7. Monitoring autophagic clearance of FL-Tau aggregates. A-C) All SH-cells were incubated O/N and treated with Bafilomycin (Baf, 320 nM, Sigma), or left untreated, for 3 H before fixation and saponin permeabilization. Next, cells were stained with Hoechst, with primary antibody recognizing p62, LC3, TAX1BP1 and LAMP1, and with fluorescent conjugate secondary antibodies. Images are confocal pictures (63 x, zoom 1.6, px size= 60nm) representative of 3 independent experiments for p62 / LC3 / FL-Tau and of 1 independent experiment for TAX1BP/ FL-Tau and LAMP1/ LC3 / FL-Tau. Scale bar 10 um. In A arrows point colabeling of p62 and LC3; arrowheads point colabeling of p62 / LC3 / FL-Tau. In B arrows point colocalization of TAX1BP/ FL-Tau. In C arrows point colocalization of LAMP1 and LC3.

5. DISCUSSION

Tauopathies are NDs all featured by the presence of Tau aggregates, with AD being the most prevalent one. Interestingly, these diseases are very heterogenous in terms of aggregates morphology and affected cell types. For example, AD mainly presents NFTs within neurons, while PSP and CBD present tau pathology mainly within astrocytic and oligodendroglial cells (Jiang and Bhaskar, 2020). However, in all cases Tau aggregates can propagate in patients' brain following a prion-like mechanism (Guo et al., 2017), with Tau' RD domain being responsible for aggregation. Moreover, it has been proved that several tauopathies share also defects in the cellular clearance mechanisms, such as the autophagy-lysosomal pathway (Jiang and Bhaskar, 2020). Thence, one could speculate that deficits in autophagy, that selectively removes pathological Tau forms, could play a relevant role into accumulation of Tau aggregates. On the other hand, one cannot exclude that Tau aggregates are themselves responsible for autophagic defects in tauopathies.

During my internship, I attempted to understand whether Tau aggregates could affect autophagic flux and whether they are substrate of autophagic clearance. To address these points, I used a neuronal cell model of neuroblastoma SH-SY5Y cells expressing FL-Tau aggregates. These cells were generated starting from clones expressing soluble FL-Tau1N4R (P301S)-mclover3 under control of a Tet-off promoter and treated with preformed human Tau fibrils (K18 -ATTO 594) to convert soluble FL-Tau into insoluble FL-Tau aggregates.

Aiming to understand if FL-Tau aggregates could influence autophagy, I monitored autophagic flux by LC3 and p62 immunoblot, respectively used as marker for autophagosomes and for selective substrate, both in presence and in absence of bafilomycin (Baf). Protein levels were monitored in cells grown for 3 hours in optimal condition or in serum-starvation.

Firstly, serum-starvation was expected to enhance autophagy. However, my findings showed that 3H-starvation did not produce the expected outcomes, probably due to its short duration (**Fig. 5A**). Therefore, starvation should be prolonged to increase autophagic flux and activity. As instance, previous reports

showed that serum-starvation for 12/24H ensures enhancement of autophagy in SH-SY5Y cells (Mohan et al., 2011).

Concerning autophagic flux in optimal condition, LC3-immunoblot results showed that all SH-cells exhibited a difference of LC3-II levels between Baf-treated and untreated samples, meaning that in all cells autophagosomes are generated and delivered to lysosomes for degradation. Thus, we could presume that FL-Tau aggregates are not compromising the flux. In fact, if FL-Tau aggregates had impaired autophagic flux, H9A10 cells would have had equal levels of LC3-II in presence and in absence of the inhibitor.

Potential influence of FL-Tau aggregates on autophagic activity was tested by comparing LC3-II/loading control ratio among Baf-treated samples. Results showed that LC3-II levels were higher in both cells expressing soluble FL-Tau, giving the impression that soluble FL-Tau and not FL-Tau aggregates could enhance formation of autophagosomes in these cells.

Confocal visualization of LC3 in Baf-treated and untreated cells was performed to further monitor FL-Tau aggregates effects on autophagic flux and activity (**Fig. 7A**). Results confirmed those obtained by immunoblot assay. Indeed, in all Baf-treated SH-cells LC3 puncta were more numerous than in untreated cells, implying that Baf inhibited autophagosome-lysosome fusion and that in all cells there is autophagic flux. Moreover, comparing LC3-puncta among all Baf-treated and untreated samples, they were mildly higher in cells overexpressing soluble FL-Tau compared to control, suggesting that soluble FL-Tau could potentially enhance autophagic activity by inducing autophagosome synthesis. However, one could question whether soluble FL-Tau is responsible for accumulation of LC3 since increase of autophagic activity seen as accumulation of p62 was showed to be a clonal effect rather than due to overexpression of soluble FL-Tau (**Fig 6B/D**). Western blot of LC3 in Dox-treated C5 cells could help to clarify this point.

Regarding p62, immunoblot in optimal condition showed that, different from controls, cells expressing soluble FL-Tau had similar amount of p62 in presence and in absence of Baf. Equal levels of p62 could have been interpreted as suppression of autophagy. However, p62 confocal results did not reproduce the equal amount of p62 between Baf-treated and untreated cells in C5 and H9A10 cells, therefore showing presence of flux which is in line with LC3 data.

Besides, both western blot and IF showed higher levels of p62 in Baf-treated cells overexpressing FL-Tau. These results seemed to validate enhancement of autophagic activity as previously seen by higher levels of LC3. One possible explanation for the positive correlation between p62 and LC3 is that p62 could initiate autophagosome biogenesis by acting as platform (Kageyama et al., 2021).

Undoubtedly, my immunoblot results should be repeated to have at least 3 independent experiments and to carry out statistical analysis. Moreover, a through quantitative analysis of LC3 and p62 puncta observed by fluorescence microscopy, should be performed before drawing any strong conclusions. Unfortunately, it was not possible to do due to lack of time.

However, from my data it seemed that soluble FL-Tau is not affecting the flux and it is not clear whether it is responsible for autophagic induction. Moreover, they would encourage to exclude any potential effect of FL-Tau aggregates on autophagic flux and activity.

Additional methods could be exploited to validate these data. To date, a powerful method is the mRFP-GFP-LC3 tandem fluorescent probe (tfLC3), as it allows to estimate both autophagic activity and flux without the use of a potentially toxic inhibitor. The GFP fluorescent signal is quenched by the acidic pH inside the lysosome, whereas mRFP signal remains stable. Thus, colocalization of GFP and mRFP fluorescence would result in yellow puncta and indicate that the tandem protein localizes in autophagosome. On the contrary, red puncta would indicate delivery of tfLC3 into lysosomes and thus formation of autophagolysosomes. To determine the autophagic flux, the relative abundance of red versus yellow puncta would be compared, with an increase in yellow puncta in case of block of autophagic flux. Induction of autophagy would result in increase of both red and yellow puncta, while inhibition of autophagy would be shown by a decrease in yellow and red puncta (Zhang et al., 2016). However, this approach would not completely fit our experimental model as it would be difficult to discriminate green FL-Tau aggregates from the TfLC3; moreover, transfection efficiency for SH-SY5Y is quite low (40-60%).

Previous data obtained in the lab by P. Chastagner and C. Brou showed that in SH-SY5Y cells endogenous RD-Tau aggregates were stable overtime, being able to

escape autophagy and proteasome degradation (Chastagner et al., 2020). Here, I wanted to investigate whether in SH cells FL-Tau aggregates behave the same.

To test FL-Tau aggregates' stability, levels of soluble FL-Tau were reduced to avoid formation of new fibrils which would have hindered stability assessment by replacing potentially degraded ones. Once formation of new fibrils was prevented, previously formed aggregates could have been detected if not degraded. To do so, I exploited Doxycline (Dox), an antibiotic belonging to the tetracycline family, which abolished expression of soluble FL-Tau, that in my neuronal cell model was under the control of a Tetracyclin(TET)-off promoter.

For achieving this aim, proteins were extracted from cells containing soluble FL-Tau daily treated with Dox or left untreated. The soluble fraction (containing soluble FL-Tau) was separated from the insoluble one (containing insoluble FL-Tau aggregates) and both transferred to a PVDF membrane, eventually incubated with GFP primary antibody, able to recognize the fluorescent portion of FL-Tau(-mclover3) (**Fig. 6A**). Stable levels of soluble FL-Tau were predicted in absence of Dox and decreased ones in response to Dox, starting form the third day of treatments as already seen by Christel Brou (data not showed).

Despite not following the expected trend, soluble FL-Tau was expressed in untreated C5 cells, and it decreased in response to Dox (**Fig. 6B/C**). Not-surprisingly, cells expressing aggregates showed very low levels of soluble FL-Tau (**Fig. 6D**), which forms fibrils soon after it is synthesized. Unexpectedly, similar levels of insoluble material were found in Dox-treated and untreated C5 cells (**Fig. 6C**). A possible explanation is formation of insoluble oligomers from overexpressed protein. However, I would have expected less material in cells were the antibiotic reduced soluble FL-Tau. Concerning FL-Tau aggregates, they were present over time in untreated cells, although not at constant levels as predicted. Contrariwise, in Dox-treated cells aggregates seemed to decrease already at D1, possibly because of lower levels of soluble FL-Tau which reduced generation of new fibrils. However, FL-Tau aggregates were no longer detected in the following days (**Fig. 6D/E**), when synthesis of new aggregates was supposed to be already turned off, conveying the impression that FL-Tau aggregates were potentially degraded. This hypothesis was further supported by IF results, were FL-Tau aggregates seemed to be cleared at day six of treatment (**Fig. 6F**). Despite that,

when comparing H9A10 to C5 cells, sharp increase of insoluble material compared to the soluble one in H9A10 cells strongly supported that in these cells FL-Tau is more stable in its aggregated form than in the soluble one.

Clearly, these data should all be repeated in the future as the experiment was performed only once. Moreover, counting the number of aggregates per cell by using computer software, like Icy, would have given a better picture of what is regarding aggregates degradation. Yet, due to lack of time this was not possible to be performed.

Nonetheless, from my observations one could presume that FL-Tau aggregates were not stable for more than several days, suggesting that these neuroblastoma cells are equipped with mechanisms able to degrade these aggregates. In addition, one could claim that cell division could have diluted aggregates between the increasing number of cells. However, if aggregates were stable enough one should have detected some in each cell, which was not the case after 6 days (IF).

One limitation of this experiment was the loading control, which prevented an accurate protein quantification and comparisons between samples. To overcome this issue, a solution would be increasing the starting amount of cell pellet to ease loading the same amount of protein. Then, GAPDH (or actin) could be exploited again as control for the soluble fraction, whereas p62-levels could be used for the insoluble one since they were showed not be affected by Dox-treatment. Doubtless, more experiments could be carried out to deepen aggregates stability. In fact, next I will perform a qPCR to further validate reduction of FL-Tau expression in Dox-treated cells. Moreover, it would be of great interest to monitor FL-Tau aggregates' fate by performing live-cell analysis through the IncuCyte system, which would allow visualization and quantification of aggregates over time.

To evaluate the participation of autophagy in potential FL-Tau degradation, I monitored their association with autophagic receptors, autophagosomes and lysosomes. For colocalization assay, cells were treated with Baf to observe receptors and autophagosomes, otherwise degraded by autophagy itself. Then, cells were incubated with antibodies against p62, TAX1BP1, LC3 and LAMP1, and analyzed by confocal microscopy.

Qualitative analysis of IF data suggested that in all SH cells there was a good colocalization between p62 and LC3 (**Fig 7A**) and between LC3 and LAMP1 (**Fig 7C**). Consistently, this could imply that the autophagic receptor was recruited by autophagosomes and that they were delivered to lysosomes, in accordance with these cells undergoing autophagic flux as already showed from my previous data.
However, although very few FL-Tau aggregates were colabelling with receptors, most of them seemed not to be labeled by the autophagy adapter p62 (**Fig 7A**) nor by TAX1BP1 (**Fig 7B**), in agreement with the fact that these two receptors are supposed to colocalize, being part of the same complex (Simonsen and Wollert, 2022). Besides, FL-Tau aggregates looked not to associate neither with autophagosomes nor with lysosomes. In addition, it seemed that under Baf-inhibitory condition number of aggregates per cell remained stable (**Supp. 1B**). On the other hand, if aggregates were substrates of autophagic clearance, I would have expected to see an increase of number of aggregates per cells in response to Baf.

Undoubtedly, it is not possible to draw any strong conclusion since not all the experiments were replicated and no statistical analysis was performed. In fact, my data needed quantification of the degree of colocalization between aggregates and the investigated autophagic proteins, by for example calculating the Pearson correlation coefficient (PCC) and the Mander's overlap coefficient (MOC). In addition, quantification of the number of aggregates in presence and in absence of Baf would have elucidated aggregates degradation. Yet, quantifications were not performed due to lack of time.

Nonetheless, my observations conveyed the impression that FL-Tau aggregates were potentially recognized as species to be cleared, but their autophagic clearance was not completed. Moreover, lack of degradation by autophagy was supported by aggregates' number stability upon autophagy inhibition.
In case quantitative data confirm that FL-Tau aggregates and p62/TAX1BP1 do not associate, it would be interesting to speculate whether FL-Tau aggregates could be recognized by other receptors, such as OPTN, which was previously shown to be found in NFTs in AD brains (Osawa et al., 2011). Moreover, if future experiments confirm that FL-aggregates are degraded in an autophagic-independent manner, one could question whether degradation occurs through proteasome. A fast approach would be analyzing the number of aggregates in cells upon proteasome inhibitors,

such as bortezomide, which should induce accumulation of aggregates in case of proteasomal degradation.

Despite further proves are needed, from my qualitative data one could presume that FL-Tau and RD-Tau have different fates. In fact, Chastagner et al., 2020 showed that in SH cells RD-Tau aggregates' autophagic degradation was partially blocked, in accordance with accumulation of autophagic vesicles in AD brain (Nixon et al., 2005). Besides, RD-Tau aggregates were colabeled with p62 and ubiquitin, in line with what observed in neurons of AD patients, where a subset of NFTs contained p62 and were ubiquitinated (Li et al., 2022). Finally, they showed that these aggregates were stable, consistent with accumulation of NFTs in AD brains (Blaudin de Thé et al., 2021). All these elements made their SH cells expressing RD-Tau aggregates a good model to study tauopathies.

On the contrary, my observations suggested that in SH cells FL-Tau aggregates were likely not to affect autophagic flux, nor to be recognized by p62 nor to be degraded by autophagy. However, only further validations and data quantification would confirm if SH cells expressing FL-Tau behave differently from SH cells expressing RD-Tau.

Moreover, from a general overview of this study it was possible to notice that H9A10, expressing both FL-Tau aggregates and soluble FL-Tau, did not show any difference with C5 cells, overexpressing only soluble FL-Tau. This means that, any potential change in autophagic flux or autophagic activity would have resulted from overexpressed soluble Tau rather than from presence of FL-Tau aggregates. Therefore, an interesting aspect of this study is that C5 cells could represent a suitable model to study the first steps of tauopathies. Indeed, overexpressed soluble Tau could form small Tau oligomers, which appear inside neurons at the early stages of AD. Interestingly, these oligomers have been shown to play a key role in neuronal loss compared to NFTs, which are thought to be probably neither sufficient nor necessary to induce neuronal dysfunction and toxicity (Niewiadomska et al., 2021).

Collectively, these preliminary data emphasized the importance of finding an appropriate neuronal cell model to solve the controversial relationship between Tau aggregates and autophagic defects in tauopathies.

6. SUPPLEMENTARY MATERIAL

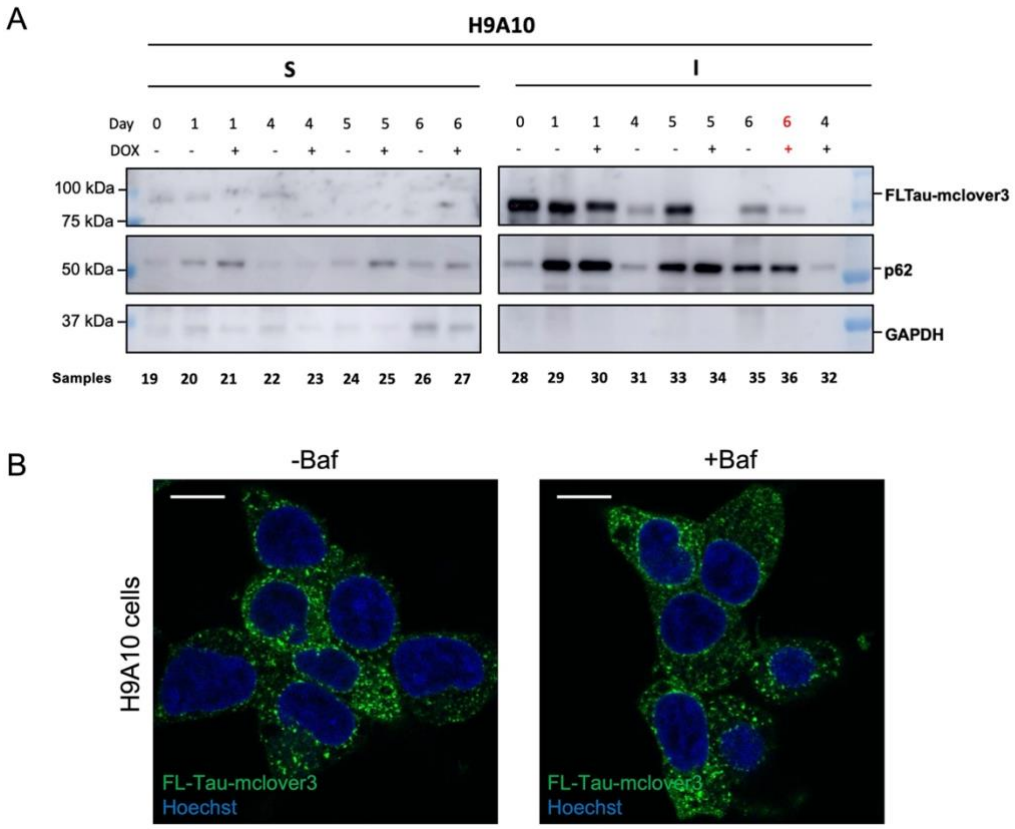

Supplementary figures 1. A) Original membrane of p62 and LC3 immunoblot in H9A10 cells. **B)** H9A10 cells were incubated O/N and treated with Bafilomycin (Baf, 320 nM, Sigma), or left untreated, for 3 H before fixation, saponin permeabilization and staining with Hoechst. Images are confocal pictures (63 x, zoom 1.6, px size= 60nm) representative of 3 independent experiments.

7. REFERENCES

1. Blaudin de Thé FX, Lassus B, Schaler AW, Fowler SL, Goulbourne CN, Jeggo R, Mannoury la Cour C, Millan MJ, Duff KE. P62 accumulates through neuroanatomical circuits in response to tauopathy propagation. Acta Neuropathol Commun. 2021 Nov 2;9(1):177. doi: 10.1186/s40478-021-01280-w. PMID: 34727983; PMCID: PMC8561893.
2. Braak H, Braak E. Neuropathological stageing of Alzheimer-related changes. Acta Neuropathol. 1991;82(4):239-59. doi: 10.1007/BF00308809. PMID: 1759558.
3. Braak H, Thal DR, Ghebremedhin E, Del Tredici K. Stages of the pathologic process in Alzheimer disease: age categories from 1 to 100 years. J Neuropathol Exp Neurol. 2011 Nov;70(11):960-9. doi: 10.1097/NEN.0b013e318232a379. PMID: 22002422.
4. Chastagner P, Loria F, Vargas JY, Tois J, I Diamond M, Okafo G, Brou C, Zurzolo C. Fate and propagation of endogenously formed Tau aggregates in neuronal cells. EMBO Mol Med. 2020 Dec 7;12(12):e12025. doi: 10.15252/emmm.202012025. Epub 2020 Nov 12. PMID: 33179866; PMCID: PMC7721367.
5. Chen W, Shen T, Wang L, Lu K. Oligomerization of Selective Autophagy Receptors for the Targeting and Degradation of Protein Aggregates. Cells. 2021 Aug 5;10(8):1989. doi: 10.3390/cells10081989. PMID: 34440758; PMCID: PMC8394947.
6. Guillozet AL, Weintraub S, Mash DC, Mesulam MM. Neurofibrillary tangles, amyloid, and memory in aging and mild cognitive impairment. Arch Neurol. 2003 May;60(5):729-36. doi: 10.1001/archneur.60.5.729. PMID: 12756137.
7. Guo T, Noble W, Hanger DP. Roles of tau protein in health and disease. Acta Neuropathol. 2017 May;133(5):665-704. doi: 10.1007/s00401-017-1707-9. Epub 2017 Apr 6. PMID: 28386764; PMCID: PMC5390006.
8. Holtzman DM, Morris JC, Goate AM. Alzheimer's disease: the challenge of the second century. Sci Transl Med. 2011 Apr 6;3(77):77sr1. doi: 10.1126/scitranslmed.3002369. PMID: 21471435; PMCID: PMC3130546.
9. Jiang S, Bhaskar K. Degradation and Transmission of Tau by Autophagic-Endolysosomal Networks and Potential Therapeutic Targets for Tauopathy. Front Mol Neurosci. 2020 Oct 16;13:586731. doi: 10.3389/fnmol.2020.586731. PMID: 33177989; PMCID: PMC7596180.
10. Kageyama S, Gudmundsson SR, Sou YS, Ichimura Y, Tamura N, Kazuno S, Ueno T, Miura Y, Noshiro D, Abe M, Mizushima T, Miura N, Okuda S, Motohashi H, Lee JA, Sakimura K, Ohe T, Noda NN, Waguri S, Eskelinen EL, Komatsu M. p62/SQSTM1-droplet serves as a platform for autophagosome formation and anti-oxidative stress response. Nat Commun. 2021 Jan 4;12(1):16. doi: 10.1038/s41467-020-20185-1. PMID: 33397898; PMCID: PMC7782522.
11. Klionsky DJ et al. Guidelines for the use and interpretation of assays for monitoring autophagy (3rd edition). Autophagy. 2016;12(1):1-222. doi: 10.1080/15548627.2015.1100356. Erratum in: Autophagy. 2016;12(2):443. Selliez, Iban [corrected to Seiliez, Iban]. PMID: 26799652; PMCID: PMC4835977.

12. Li L, Jiang Y, Wang JZ, Liu R, Wang X. Tau Ubiquitination in Alzheimer's Disease. Front Neurol. 2022 Feb 8;12:786353. doi: 10.3389/fneur.2021.786353. PMID: 35211074; PMCID: PMC8860969.
13. Lim S, Haque MM, Kim D, Kim DJ, Kim YK. Cell-based Models To Investigate Tau Aggregation. Comput Struct Biotechnol J. 2014 Oct 2;12(20-21):7-13. doi: 10.1016/j.csbj.2014.09.011. PMID: 25505502; PMCID: PMC4262059.
14. Ma S, Attarwala IY, Xie XQ. SQSTM1/p62: A Potential Target for Neurodegenerative Disease. ACS Chem Neurosci. 2019 May 15;10(5):2094-2114. doi: 10.1021/acschemneuro.8b00516. Epub 2019 Apr 19. PMID: 30657305; PMCID: PMC6712989.
15. Mohan N, Banik NL, Ray SK. Combination of N-(4-hydroxyphenyl) retinamide and apigenin suppressed starvation-induced autophagy and promoted apoptosis in malignant neuroblastoma cells. Neurosci Lett. 2011 Sep 8;502(1):24-9. doi: 10.1016/j.neulet.2011.07.016. Epub 2011 Jul 20. PMID: 21801811; PMCID: PMC3159706.
16. Nakatogawa H. Mechanisms governing autophagosome biogenesis. Nat Rev Mol Cell Biol. 2020 Aug;21(8):439-458. doi: 10.1038/s41580-020-0241-0. Epub 2020 May 5. PMID: 32372019.
17. Nakayama Y, Sakamoto S, Tsuji K, Ayaki T, Tokunaga F, Ito H. Identification of linear polyubiquitin chain immunoreactivity in tau pathology of Alzheimer's disease. Neurosci Lett. 2019 Jun 11;703:53-57. doi: 10.1016/j.neulet.2019.03.017. Epub 2019 Mar 15. PMID: 30885635.
18. Niewiadomska G, Niewiadomski W, Steczkowska M, Gasiorowska A. Tau Oligomers Neurotoxicity. Life (Basel). 2021 Jan 6;11(1):28. doi: 10.3390/life11010028. PMID: 33418848; PMCID: PMC7824853.
19. Nixon RA, Wegiel J, Kumar A, Yu WH, Peterhoff C, Cataldo A, Cuervo AM. Extensive involvement of autophagy in Alzheimer disease: an immuno-electron microscopy study. J Neuropathol Exp Neurol. 2005 Feb;64(2):113-22. doi: 10.1093/jnen/64.2.113. PMID: 15751225.
20. Osawa T, Mizuno Y, Fujita Y, Takatama M, Nakazato Y, Okamoto K. Optineurin in neurodegenerative diseases. Neuropathology. 2011 Dec;31(6):569-74. doi: 10.1111/j.1440-1789.2011.01199.x. Epub 2011 Feb 1. PMID: 21284751.
21. Peller P, Murphy R, Subramaniam R, Journal of Nuclear Medicine May 2009, 50 (supplement 2) 1081.
22. Silva MC, Nandi GA, Tentarelli S, Gurrell IK, Jamier T, Lucente D, Dickerson BC, Brown DG, Brandon NJ, Haggarty SJ. Prolonged tau clearance and stress vulnerability rescue by pharmacological activation of autophagy in tauopathy neurons. Nat Commun. 2020 Jun 26;11(1):3258. doi: 10.1038/s41467-020-16984-1. PMID: 32591533; PMCID: PMC7320012.
23. Scrivo A, Bourdenx M, Pampliega O, Cuervo AM. Selective autophagy as a potential therapeutic target for neurodegenerative disorders. Lancet Neurol. 2018 Sep;17(9):802-815. doi: 10.1016/S1474-4422(18)30238-2. PMID: 30129476; PMCID: PMC6359907.
24. Simonsen A, Wollert T. Don't forget to be picky - selective autophagy of protein aggregates in neurodegenerative diseases. Curr Opin Cell Biol. 2022 Feb 28;75:102064. doi: 10.1016/j.ceb.2022.01.009. Epub ahead of print. PMID: 35240373.

25. Wang Y, Martinez-Vicente M, Krüger U, Kaushik S, Wong E, Mandelkow EM, Cuervo AM, Mandelkow E. Tau fragmentation, aggregation and clearance: the dual role of lysosomal processing. Hum Mol Genet. 2009 Nov 1;18(21):4153-70. doi: 10.1093/hmg/ddp367. Epub 2009 Aug 4. PMID: 19654187; PMCID: PMC2758146.
26. Takashima et al. (eds.), Tau Biology, Advances in Experimental Medicine and Biology 1184, https://doi.org/10.1007/978-981-32-9358-8_1 Springer Nature Singapore Pte Ltd. 2019.
27. Tan JM, Wong ES, Kirkpatrick DS, Pletnikova O, Ko HS, Tay SP, Ho MW, Troncoso J, Gygi SP, Lee MK, Dawson VL, Dawson TM, Lim KL. Lysine 63-linked ubiquitination promotes the formation and autophagic clearance of protein inclusions associated with neurodegenerative diseases. Hum Mol Genet. 2008 Feb 1;17(3):431-9. doi: 10.1093/hmg/ddm320. Epub 2007 Nov 1. PMID: 17981811.
28. Vogels T, Leuzy A, Cicognola C, Ashton NJ, Smolek T, Novak M, Blennow K, Zetterberg H, Hromadka T, Zilka N, Schöll M. Propagation of Tau Pathology: Integrating Insights From Postmortem and In Vivo Studies. Biol Psychiatry. 2020 May 1;87(9):808-818. doi: 10.1016/j.biopsych.2019.09.019. Epub 2019 Oct 3. PMID: 31735253.
29. Zhang Z, Singh R, Aschner M. Methods for the Detection of Autophagy in Mammalian Cells. Curr Protoc Toxicol. 2016 Aug 1;69:20.12.1-20.12.26. doi: 10.1002/cptx.11. PMID: 27479363; PMCID: PMC4982470.

8. ACKNOWLEDGEMENTS

I would like to thank Chiara Zurzolo, the head of the lab, for having provided me with the opportunity to work in a such collaborative, stimulating and creative environment. This experience extremely helped me to grow both from a scientific and a personal point of view. I would like to express my gratitude to Chistel Brou, my supervisor, for the patient, the encourage and all the advice she gave me during these months. A special thank for taking care about my project and for being always present to solve my doubts. From the bottom of my heart, I would like to say a big thank to all the other members of the group for their energy, personal support and for creating a pleasant atmosphere in the lab.

Thank also to University of Padua which allowed me to take part of the Double Degree program and to Professor Chiara Rampazzo for supervising my work.

Naturalmente inizio ringraziando voi, Andrea, Linda, Elena, Michela, Lucia, Gaia. La prima cosa che mi viene da dire è grazie per aver creato un gruppo così coeso e affiatato. Grazie per tutte le cene in camera e quelle fuori con The Fork, per le passeggiate per Parigi, per i picnic sulla Senna, per i pains au chocolate nei momenti no, per le confessioni sul letto con la tisana, per i karaoke in camera, per i nostri viaggetti, e tanto altro. Non c'è stato giorno in cui io mi sia sentita sola, siete sempre corsi da me ogni volta che ne avevo bisogno: per sentirmi ripetere, per portarmi la spesa, per abbracciarmi quando ne avevo bisogno, per prepararmi la cena quando non avevo tempo.. e anche per dire qualche cavolata via!
Ci tengo a sottolineare che insieme a voi io, persona perennemente insoddisfatta e alla continua ricerca di altro, non ho mai sentito il bisogno di altro. *Mi avete dato tutto quello di cui avevo bisogno*.

Grazie Andre per il tuo cuore grande, non dimenticherò tutto quello che hai fatto pur di ascoltare il mio discorso prima della laurea. Sono fiera di te, del fatto che hai resistito alla "convivenza" con sei scellerate, ma soprattutto dell'uomo che sei diventato. E.. grazie per la tua pasta con le acciughe.. spiciale!

Grazie Michi per avermi guidato verso la giusta strada, non solo nella burocrazia, ma anche nella riservatezza e per avermi fatto capire che fare le cose da

soli ha un sapore diverso. Tu così silenziosa, ma così presente. Porto sempre con me la frase che mi dissi a marzo: "Elo, non sono brava con le parole, ma sappi che se hai bisogno sono qui per ascoltarti". Sei stata una bella scoperta.

Grazie Ele, per aver portato sempre gioia nel gruppo, con il tuo sorriso, la tua spensieratezza, la tua gioia, la tua curiosità per la vita e per ciò che hai attorno. Tu che non ti sei mai lamentata di nulla, anche quando avresti potuto farlo, mi hai trasmesso leggerezza e allegria. Grazie per non avermi mai fatto mancare il dolce dopo cena, tu si che sei un'amica (bascioni).

Grazie Luci, perché per me sei un esempio di intelligenza, scaltrezza, creatività, simpatia, bellezza e umiltà. Sei una persona che ha tutte le carte in regola per spaccare il mondo e per ottenere tutto quello che desideri nella vita. Hai un potenziale che non ti immagini. È stato un onore lavorare con te, ma ancora di più è stato un piacere essere stata la tua fida per un mesetto (sorry Dà!).

Grazie Gaia, perché mi hai fatto capire quanto è bello essere appassionati per qualcosa, quanto è bello importante avere talenti diversi, quanto è fondamentale inseguire quello che ci piace nonostante qualcuno non ci appoggi. Mi raccomando, non perdere di mira il tuo obiettivo (e magna!).

Infine, grazie a Linda, la mia gemella (diversa). Non so da dove iniziare, ne avrei così tante da dire. Ti ringrazio per avermi dimostrato quanto trovare il giusto equilibrio contribuisca alla nostra serenità. La calma e la purezza che trasmetti derivano dal fatto che tu hai trovato il giusto compresso in molti ambiti della tua vita: tra lo studio ed il piacere, tra il dire la verità e il non offendere, tra il dedicare tempo agli altri e a te stessa.. Ti ringrazio per esserci sempre stata, per avermi lasciato piangere, per ascoltarmi, per avermi dato consigli preziosi e per avermi fatto ridere in giornate buie. Grazie per le passeggiate mattutine, andare al lavoro con te rendeva la giornata più energica. Grazie per avermi detto "No Elo, it's time to grow!" e per avermi accettato così come sono e per aver assecondato tutte le mie piccole follie. È stato bello condividere questa esperienza con te e, soprattutto, il momento in cui ci siamo impresse sulla pelle la gioia che ci ha portato.

Cari amici, siete delle persone spettacolari.
Grazie di nuovo per tutto quello che avete fatto per me.
Vi voglio bene.

Un grazie anche a Margherita, Giovanna, Francesco, Francesca, Francesca, Riccardo e tutti i ragazzi di Padova che hanno alleggerito il mio primo anno di magistrale con le loro birrette e le loro cenette.
Un grazie alle mie amiche storiche di Viterbo Carlotta, Giulia, Francesca, Martina per essere sempre con me ovunque io mi trovi.
Un grazie a Roberta, Giorgia, Nadia e Francesca, le persone più dolci del mondo, che anche a distanza riescono incredibilmente ad essere presenti.

Infine, un enorme grazie alla mia famiglia, la cosa più preziosa che ho. Grazie mamma e papà, perché per ben 25 anni mi avete dato libertà, fiducia, e supporto. Grazie perché siete riusciti a creare una Casa fatta di amore, unione, ma anche di litigi, sacrifici, lavoro e indipendenza. Una Casa in cui non è mai mancato nulla (se non la nutella), in cui non si avverte l'esigenza di *andarsene*, ma piuttosto il piacere di *tornare*. Non smetterò mai di esservi grata per farmi vivere la vita più bella che si possa desiderare. Grazie perché siete esattamente l'esempio di quello che io voglio nella vita.
Grazie alle persone che più amo al mondo, i miei fratelli, per farmi quotidianamente capire che la diversità non è un limite, ma anzi è una ricchezza.